Torque vectoring using e-axle configuration for 4WD battery electric truck

Utilizing control allocation for motion control and steer by propulsion

Master's thesis in Systems, Control and Mechatronics

Emil Fahlgren
Daniel Söderberg

DEPARTMENT OF MECHANICS AND MARITIME SCIENCES
CHALMERS UNIVERSITY OF TECHNOLOGY
Gothenburg, Sweden 2022
www.chalmers.se

Master's thesis 2022:24

Torque vectoring using e-axle configuration for 4WD battery electric truck

Utilizing control allocation for motion control and steer by propulsion

Emil Fahlgren
Daniel Söderberg

Department of Mechanics and Maritime Sciences
Division of Vehicle Engineering and Autonomous Systems
Vehicle Dynamics Group
Chalmers University of Technology
Gothenburg, Sweden 2022

Torque vectoring using e-axle configuration for 4WD battery electric truck
Utilizing control allocation for motion control and steer by propulsion
EMIL FAHLGREN
DANIEL SÖDERBERG

Supervisor: Leo Laine & Sachin Janardhanan, Volvo Group Trucks Technology, Gothenburg, Sweden
Examiner: Mats Jonasson, Mechanics and Maritime Sciences, Chalmers University of Technology, Gothenburg, Sweden

Master's thesis MMSX30 / 2022:24
Department of Mechanics and Maritime Sciences
Division of Vehicle Engineering and Autonomous Systems
Vehicle Dynamics Group
Chalmers University of Technology
SE-412 96 Gothenburg
Telephone +46 31 772 1000

Typeset in LaTeX
Printed by Chalmers Reproservice
Gothenburg, Sweden 2022

Torque vectoring using e-axle configuration for 4WD battery electric truck
Utilizing control allocation for motion control and steer by propulsion
EMIL FAHLGREN
DANIEL SÖDERBERG
Department of Mechanics and Maritime Sciences
Chalmers University of Technology

Abstract

With the rise of electric drives in vehicle applications, configurations of new powertrain design are emerging. In recent years, this trend has shifted to include heavy vehicles as well. In this thesis, a concept 4x4 battery electric truck with a distributed powertrain is investigated. By using four individual motors on two separate e-axles, different coordination possibilities are available for motion control of the truck. This thesis focuses on using torque vectoring as a principle to allocate the requested global torque. Furthermore, a novel method mentioned to as steer by propulsion (SBP) is proposed, where the steering of the vehicle can be controlled solely by using the electric machines on the front axle. Investigations are conducted to explore the effectiveness of this method on vehicle performance and energy consumption.

To distribute the control requests across the available actuators, control allocation (CA) is used. Here, the problem is formulated as a quadratic programming (QP) problem. High level controllers provide the requested global forces as an input to the control allocation, which in turn allocates torques to the separate wheel controllers. Furthermore, different formulations of the control allocator and motion controller are presented and compared.

The control system is simulated with a vehicle model provided by Volvo, and the results indicate that steer by propulsion is able to follow a reference path with a lateral offset of a magnitude of an acceptable level. Furthermore, the simulations show that SBP can repeat this behavior at high speeds as well with an oscillatory behavior. Therefore, the method is recommended to use mainly at vehicle speeds below 50 km/h. Finally, simulations show that SBP increases the energy consumption by 2-4 %. Considering that the consumption is on par with using power steering, SBP will be viable for redundancy with some limitations.

Keywords: Control system design, optimal control, control allocation,
steer by propulsion, optimization, electric powertrains,
e-axles, battery electric trucks

Acknowledgements

This master thesis was carried out at Volvo Group Trucks Technology in Gothenburg during the spring of 2022.

First of all, we would like to thank our supervisors at Volvo GTT, Leo Laine and Sachin Janardhanan for providing us with very helpful advice and interesting discussions. We would also like to thank our examiner at Chalmers, Mats Jonasson, for all his advice and support regarding the administrative parts of the thesis.

Finally, we want to thank our families for supporting us in our studies all the way, helping us through tough times and celebrating our proud moments.

Emil Fahlgren & Daniel Söderberg, Gothenburg, June 2022

List of Acronyms

Below is the list of acronyms that have been used throughout this thesis listed in alphabetical order:

4WD	Four-Wheel Drive
ABS	Anti-Lock Braking System
AD	Autonomous Driving
CA	Control Allocation
DYM	Direct Yaw Moment
ECU	Electronic Control Unit
IM	Induction Motor
iXPR	individual Xternal Propulsion Request
LQR	Linear Quadratic Regulator
PI	Proportional Integral
PMSM	Permanent Magnet Synchronous Motor
SBP	Steer By Propulsion
VTM	Volvo Transport Model
QP	Quadratic Programming

Contents

List of Acronyms **ix**

List of Figures **xiii**

List of Tables **xv**

1 Introduction **1**
1.1 Background 1
1.2 Purpose 3
1.3 Scope And Limitations 4
1.4 Research Questions 4

2 Vehicle Modeling **5**
2.1 Vehicle Dynamics 5
2.1.1 Modeling For Concept Analysis 5
2.1.2 Rigid Body Modeling 6
2.1.3 Single Track Model 8
2.2 Tire Modeling 8
2.2.1 Tire Slip 9
2.2.2 Tire Force Modeling 10
2.2.2.1 Linear Models 10
2.2.2.2 Magic Formula Tire Model 10
2.3 Electric Motors 11
2.3.1 PMSM - Permanent Magnet Synchronous Motors 11
2.3.2 IM - Induction Motors 12
2.3.3 Modeling of Electric Motors 12
2.4 Brake Systems 13
2.5 Steering System 13

3 Concept Vehicle Analysis **17**
3.1 Performance Analysis & Powertrain Sizing 17
3.2 Sensitivity Study 20
3.3 Control Analysis 21
3.3.1 Torque Vectoring Concept 21
3.3.2 Steer By Propulsion Concept 23

4 Control Design **25**

4.1 Control System Structure . . . 25
4.2 Path Follower . . . 26
4.3 Control Allocation . . . 27
4.3.1 General Formulation . . . 27
4.3.2 QP Formulation . . . 27
4.3.3 Actuator Dynamics Constraint . . . 28
4.3.4 Tire Force Constraint . . . 29
4.3.5 Desired Actuator Usage . . . 29
4.3.6 Dynamic Weighting . . . 30
4.4 Torque Vectoring . . . 30
4.4.1 Torque Distribution Using Control Allocation . . . 31
4.4.1.1 Motion Controller . . . 32
4.4.1.2 Control Allocation Formulation . . . 33
4.4.2 Steer By Propulsion . . . 34
4.4.2.1 Motion Control - Steering Angle Based . . . 34
4.4.2.2 Motion Control - Yaw Rate Based . . . 35
4.4.2.3 Motion Control - LQR Yaw Rate Based . . . 36
4.4.2.4 Steering Moment Limits . . . 38
4.4.2.5 Control Allocation Formulation . . . 38
4.4.2.6 Steering Angle Modification . . . 39
4.4.3 Modeling Of Energy Consumption . . . 40
4.5 Wheel Controllers . . . 40
4.5.1 Wheel Speed Control . . . 41
4.5.2 Wheel Torque Control . . . 41

5 Simulations 43
5.1 Wheel Controller Slip Performance . . . 44
5.2 Steer By Propulsion Performance . . . 45
5.2.1 Cornering Test Cases . . . 45
5.2.2 Test Scenarios Using Steering Angle-Based Approach . . . 54
5.3 Energy Consumption Comparison . . . 59

6 Conclusions 63

Bibliography 65

List of Figures

1.1 Illustration of suggested powertrain architecture. 2

2.1 Illustration of the vehicle model with parameters and forces acting on the vehicle. 6
2.2 Illustration of lateral tire slip, with δ representing the steering angle and α, the tire slip angle. 9
2.3 Magic Formula tire model for different road conditions. 11
2.4 Illustration of the motor map used for the motors on the cruise axle. . 12
2.5 Illustration of the motor map used for the motors on the startability axle. 13
2.6 Illustration of the scrub radius r_s. 14

3.1 Traction force diagram for the resistive forces. The dashed lines indicate the required traction force for different road gradients. 18
3.2 Force capabilities of the cruise axle, startability axle and combined axles illustrated together with the performance requirements specified in table 3.1. The capabilities of the axles are with gear ratios included. 19
3.3 Required traction force for different road gradients illustrated together with the powertrain capabilites of the cruise axle, startability axle and combined axles. 20
3.4 Illustration of how vehicle forces might be distributed for a regular vehicle, and how it might be distributed using torque vectoring. The arrows indicate the direction of the longitudinal and lateral force on each wheel. The ellipses indicate the magnitude of the total force on each wheel. 22
3.5 Illustration of how vehicle forces might be distributed for a regular vehicle, and how it might be distributed for a vehicle using SBP. The arrows indicate the direction of the longitudinal and lateral force on each wheel. The ellipses indicate the magnitude of the total force on each wheel. 23

4.1 A simple visualization of the control system architecture. 25
4.2 Illustration of geometry used for the implementation of the Stanley controller. 26

5.1 Longitudinal slip on each wheel. Dashed lines indicate the slip limit, which in this case is set to 0.2. 44

5.2 Corresponding torques on each wheel in the slip performance test. Blue indicates the actual output torque, while the dashed line indicates the request from the control allocator. 45
5.3 Test track for the cornering test. 46
5.4 Actual steering angle and yaw rate compared to references in the case of using steering angle-based control. 47
5.5 Actual steering angle and yaw rate compared to references in the case of using yaw rate-based control with PI. 48
5.6 Actual steering angle and yaw rate compared to references in the case of using yaw rate-based control with LQR using reference gain. 49
5.7 Actual steering angle and yaw rate compared to references in the case of using yaw rate-based control with LQR using integral action. . . . 50
5.8 Actual steering angle and yaw rate compared to references in the case of using steering angle-based control with a modified steering angle. . 51
5.9 Lateral offset for each respective control approach in the given test case. 52
5.10 Simulation of turn in constant radius of 50 m at 30 km/h. Lateral offset between the desired and actual path is seen below. 54
5.11 Motor torques in simulation of turn in constant radius of 50 m at 30 km/h. Dynamic limits are indicated by dashed lines. 55
5.12 Simulation of turn in constant radius of 100 m at 50 km/h. Lateral offset between the desired and actual path is seen below. 56
5.13 Motor torques in simulation of turn in constant radius of 100 m at 50 km/h. Dynamic limits are indicated by dashed lines. 57
5.14 Simulation of lane change at 85 km/h. 58
5.15 Motor torques of lane change at 85 km/h. 59

List of Tables

3.1 Table presenting vehicle parameters and performance requirements. . 17
3.2 Effects of changes in the roll and air drag coefficients on the total power requirements on the cruise axle at cruise speed in a 2% slope. . 20
3.3 The table shows the peak force that the startability axle can generate with a set of different gears as well as the corresponding maximal speed due to the motor being limited to a maximum motor speed. . . 21

5.1 Energy consumption in the case of a braking in a turn in constant radius R = 50 m, with initial velocity of 50 km/h. 60
5.2 Energy consumption in the case of a turn in constant radius R = 100 m at 50 km/h. 60
5.3 Energy consumption in the case of a lane change at 85 km/h. 61

1

Introduction

In this chapter, a thorough background to the project is provided. The purpose, scope and specific research questions are also presented.

1.1 Background

Electric drives has grown significantly in popularity during the last years, and aims at becoming the new standard mode of propulsion. Now the emerging trend in passenger vehicles, combined with requirements on CO_2 emissions, has led to the introduction of electric powertrains in heavy vehicles as well. Utilizing electric drives allows for more flexibility in the powertrain design, and also increases the importance of an optimal architecture since the added weight of the battery will be substantial. A distributed powertrain architecture consisting of two seperate e-axles was introduced in the predecessor to this thesis project [1], with the goal of maximizing the driving range.

The two e-axles are developed for different functionalities. An electronic control unit (ECU) coordinates the use of the motors. The startability axle consists of an induction motor (IM) placed on the rear axle. This axle is used if extra power is needed for steep inclines or rapid accelerations. For continuous driving along highways and rural roads, a cruise axle with a permanent magnet synchronous motor (PMSM) has been designed with the possibility to turn the wheels using regular electric power steering as well. The concept was evaluated for a 36 metric ton vehicle over a selected long-haul drive cycle in simulation. The results showed that a 50 % split between the power on each e-axle was optimal in the sense that it maximized the driving range capabilities. The architecture was then further developed by equipping each e-axle with an individual motor for each wheel. The suggested architecture for this thesis is thus illustrated in figure 1.1.

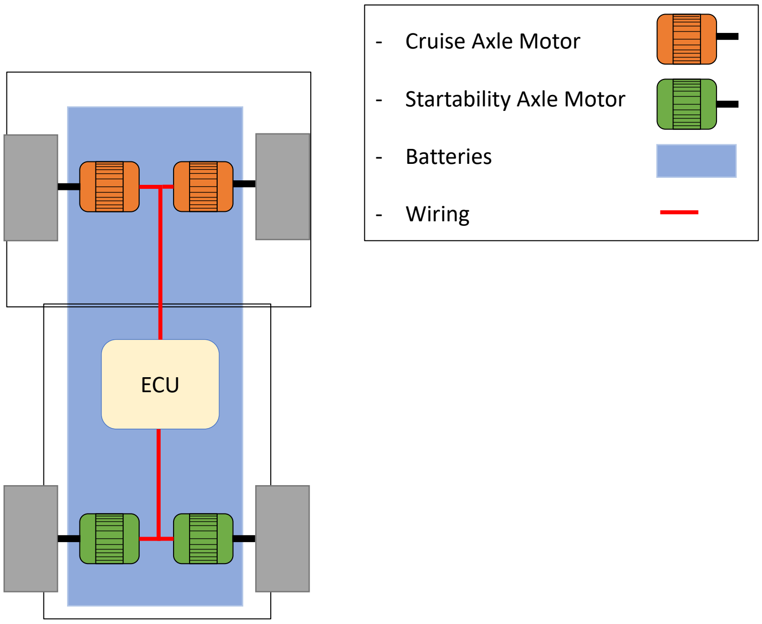

Figure 1.1: Illustration of suggested powertrain architecture.

One potential concept to minimize energy consumption is to use steer by propulsion with the electric front axle machines. During steer by propulsion, the steering mechanics of the front axle can be controlled by regulating the torque of the front electric machines. This means that the standard electric power steering can be switched off during some parts of the driving. In the case of turning, energy can potentially be saved when the electric power steering has been turned off and regenerative braking is used for one of the motors. A left turn of the truck can be achieved by using regenerative braking for the left wheel. The challenge is to perform this action in an energy efficient manner and still maintain the lateral stability of the vehicle.

The concept of having a quad-motor drive is starting to gain traction in the industry, where the American automotive manufacturer Rivian are using this design for their R1T model [2]. Another interesting model implementing a similar driveline is Tesla's Cybertruck [3]. This shows that the four-wheel drive (4WD) design for electric vehicles is growing quickly in popularity for pickup trucks.

Using individual motors for each wheel allows for torque vectoring, which means the torque on each wheel can be controlled separately. This can improve performance and efficiency in cornering maneuvers. In [4], an energy efficient torque vectoring algorithm is implemented in a SUV prototype. The simulations showed that, compared to the same vehicle with even torque distribution, this algorithm could reduce up to 4 % in power consumption in constant straight driving, and more than 5 % in steady-state cornering at lateral accelerations greater than 3.5 m/s^2. Furthermore, the algorithm helped in achieving vehicle stability in emergency conditions.

A design with four individual motors also means that the electric motors can be used to performe regenerative braking. However, regenerative braking might not be applicable in all driving situations, which means the services brakes need to intervene. Sometimes, a combination of the two could be required. In [5], torque blending is used to allocate the optimal split between the two braking mechanisms, based on energy performance metrics and more.

Using the proposed powertrain design in [1] means that the number of available actuators exceed the number of design variables in the control system. This is known as an over-actuated system, which means a combination of different actuators can be applied to obtain the desired motion. A control scheme called control allocation has been a popular choice in this scenario and has been used in similar applications as in this thesis, including works as [6] as well the predecessor to this thesis [1].

In a previous thesis at Volvo Group Trucks Technology [7], control allocation has been used for vehicle motion control of another vehicle configuration using a diesel engine. However, the vehicle modeling and control design provides beneficial insights for this thesis as well. A relevant factor that was emphasized in [7] and other papers such as [8], is tire slip. Focusing on tire slip can help stabilize the vehicle and contribute to a smoother driving experience. Methods for tire slip control can be included in the control allocation scheme for traction control of the vehicle. The configuration of the vehicle in this thesis allows for better and faster control of the separate wheels due to the fast dynamics of the motors. The slip control can therefore be achieved by the wheel controllers and hence simplify the control allocation problem.

1.2 Purpose

The purpose of this thesis is to investigate the optimal control scheme for the proposed powertrain configuration, while focusing on controlling the torque on the front axle for propelling and steering the vehicle. The performance and energy consumption of using this control strategy are the main areas of interest. Furthermore, the purpose is to analyze if this control strategy could be used to improve the redundancy of the steering system. Finally, the control design is to be evaluated for different driving situations to see if it is a feasible solution that can be used in a real-life application to achieve the desired motion and potentially minimize the energy consumption.

1.3 Scope And Limitations

- Due to a pre-determined software architecture and needed flexibility for both manual driver and autonomous driving, control allocation will be the only control strategy considered for actuator commands.
- All evaluations will be done through simulations as there is no existing prototype at the moment.
- Pre-determined motors from Volvo will be the reference used when implementing the new powertrain architecture in simulation.
- A 4x4 tractor vehicle model will be the only controlled unit in this thesis.

1.4 Research Questions

- How can the optimal control scheme be formulated for the chosen powertrain configuration, application and electric machine interface?
- How can steer by propulsion influence vehicle performance and what are its limitations?
- Compared with using power steering, how is the energy consumption affected by using steer by propulsion?

2

Vehicle Modeling

This chapter is initiated by a section on vehicle dynamics to explain how the dynamic modeling of the vehicle is done. This is followed by sections on tire dynamics, electric motors, brake systems and steering systems to cover the equations and dynamics behind the entire model. Further performance and characteristics of the powertrain configuration is investigated and demonstrated in chapter 4 where the control system for the truck is developed.

2.1 Vehicle Dynamics

In order to be able to design an optimal control system for the chosen powertrain configuration, motivate the design and analyze its performance, the dynamics of the vehicle have to be modeled. The motion of a vehicle can be described by its longitudinal, lateral and vertical dynamics. Regarding the model in this study, the vertical dynamics will be neglected for simplicity.

2.1.1 Modeling For Concept Analysis

Analyzing the longitudinal behavior serves as an appropriate starting point for further investigation and development of the concept. Newton's laws can be used to set up this model by observing the forces acting on the truck. The driving force on the vehicle is denoted as F_D and the rolling resistance is denoted as F_{RR}. Other forces acting on the vehicle is air drag F_a and gravity F_g. The longitudinal vehicle motion can be described using equations (2.1) - (2.3).

$$m\dot{v}_x = F_D - F_a - F_{RR} - F_g \tag{2.1}$$

The air drag can be calculated according to equation (2.2) where c_d is the air drag coefficient, A_f is the frontal area and ρ is the air density.

$$F_a = \frac{1}{2} c_d \rho A_f v_x^2 \tag{2.2}$$

The rolling resistance for the front and rear axle can be calculated according to equation (2.3) where c_r is the rolling resistance coefficient and F_z is the combined normal load on all wheels.

$$F_{RR} = c_r F_z \tag{2.3}$$

The gradient load of the vehicle depends on the grade of the road, θ, according to equation (2.4).

$$F_g = mg\sin(\theta) \tag{2.4}$$

2.1.2 Rigid Body Modeling

The motion of the vehicle can also be described with added complexity. This thesis considers a 3 degree of freedom planar model. Figure 2.1 illustrates the forces acting on the vehicle in the vehicle frame and the forces acting on the wheel in the wheel frame. To distinguish between forces in the vehicle frame and wheel frame, a w is added in the index for the wheel frame. The parameters T_f and T_r are the track width of each respective axle and the variables L_f and L_r are the distances from the center of mass to the vehicle axles.

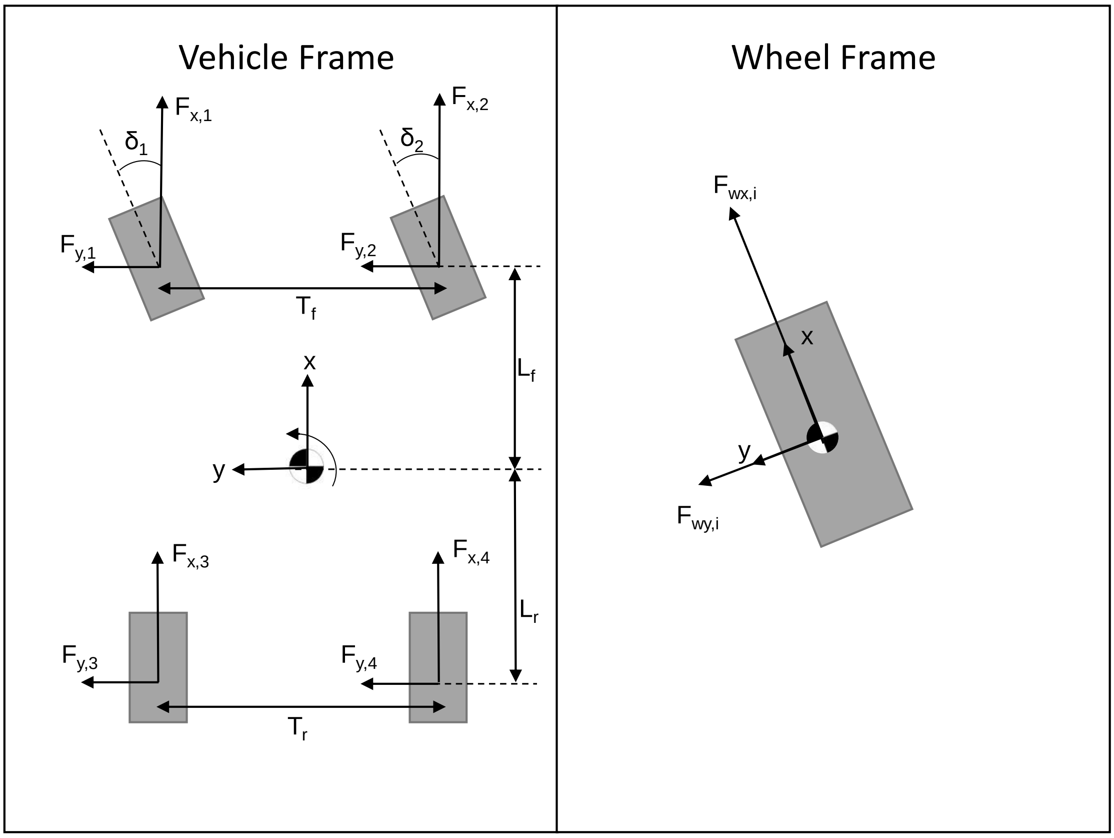

Figure 2.1: Illustration of the vehicle model with parameters and forces acting on the vehicle.

The rigid body dynamics of the vehicle can be defined according to equation (2.5) as stated in [7]. The equations consider motion with 6 degress of freedom, since only motion in the xy-plane is considered one can define $\mathbf{v} = [v_x \;\; v_y \;\; 0]^T$, $\boldsymbol{\omega} = [0 \;\; 0 \;\; \omega_z]^T$

and $\mathbf{F}_i = [F_{x,i} \;\; F_{y,i} \;\; 0]^T$.

$$m(\dot{\mathbf{v}} + \boldsymbol{\omega} \times \mathbf{v}) = \sum_i \mathbf{F}_i \tag{2.5a}$$

$$I\dot{\boldsymbol{\omega}} + \boldsymbol{\omega} \times (\boldsymbol{I\omega}) = \sum_i \mathbf{M}_i \tag{2.5b}$$

The forces that the wheels produce are later provided in the wheel frame. A rotation matrix can be used to rotate the forces to the vehicle frame according to equation (2.6).

$$\begin{bmatrix} F_{x,i} \\ F_{y,i} \end{bmatrix} = \begin{bmatrix} cos(\delta_i) & -sin(\delta_i) \\ sin(\delta_i) & cos(\delta_i) \end{bmatrix} \begin{bmatrix} F_{wx,i} \\ F_{wy,i} \end{bmatrix} \tag{2.6}$$

The forces in the x and y direction can hence be written according to equation (2.7).

$$F_{x,i} = F_{wx,i}cos(\delta_i) - F_{wy,i}sin(\delta_i) \tag{2.7a}$$

$$F_{y,i} = F_{wy,i}cos(\delta_i) + F_{wx,i}sin(\delta_i) \tag{2.7b}$$

The distance and force vector for each wheel can be expressed according to equation (2.8), where L_i and T_i are the x and y coordinates of the center of the wheel. Note that they might be negative.

$$\mathbf{r}_i = \begin{bmatrix} L_i \\ T_i/2 \\ 0 \end{bmatrix} \tag{2.8a}$$

$$\mathbf{F}_i = \begin{bmatrix} F_{x,i} \\ F_{y,i} \\ 0 \end{bmatrix} \tag{2.8b}$$

The moment around the center of mass produced by a wheel is calculated using the cross product, as shown in equation (2.9).

$$M_{z,i} = \mathbf{r}_i \times \mathbf{F}_i \tag{2.9}$$

Then, for each wheel the moment can be expressed according to equation (2.10).

$$M_{z,i} = L_i(F_{wy,i}cos(\delta_i) + F_{wx,i}sin(\delta_i)) - \frac{T_i}{2}(F_{wx,i}cos(\delta_i) - F_{wy,i}sin(\delta_i)) \tag{2.10}$$

The total forces and moments acting on the vehicle is therefore the sum of the forces produced by the wheels, according to equation (2.11).

$$F_x = \sum_i F_{x,i} \tag{2.11a}$$

$$F_y = \sum_i F_{y,i} \tag{2.11b}$$

$$M_z = \sum_i M_{z,i} \tag{2.11c}$$

Finally the equations for the rigid body dynamics are simplified according to equation (2.12) by omitting variables that are not considered, i.e. v_z, ω_x and ω_y.

$$\begin{bmatrix} m\dot{v}_x \\ m\dot{v}_y \\ I_{zz}\dot{\omega}_z \end{bmatrix} = \begin{bmatrix} mv_y\omega_z + \sum_i F_{x,i} \\ -mv_x\omega_z + \sum_i F_{y,i} \\ \sum_i M_{z,i} \end{bmatrix} \tag{2.12}$$

2.1.3 Single Track Model

The single track model of the vehicle lumps the wheels on the front and rear axles to a single wheel in the middle of each axle. The model resembles a bicycle and in this case only the front axle is steered, therefore the steering angle of the front wheel is defined as δ_f. The equations describing the motion are shown in equation (2.13). Here, δ_f is assumed to be small, such that $\cos(\delta_f) \approx 1$ and $\sin(\delta_f) \approx 0$.

$$m(\dot{v}_x - v_y\omega_z) = F_{wx,f} + F_{wx,r} \tag{2.13a}$$

$$m(\dot{v}_y + v_x\omega_z) = F_{y,f} + F_{y,r} \tag{2.13b}$$

$$I_{zz}\dot{\omega}_z = L_f F_{y,f} - L_r F_{y,r} \tag{2.13c}$$

If the vehicle is assumed to be driven at constant longitudinal velocity, the first equation can be neglected. If the body slip of the vehicle is assumed to be small and if the longitudinal velocity is constant, the body slip can be defined according to equation (2.14a). With this in mind, equation (2.13b) can be written as in equation (2.14b).

$$\beta = \frac{v_y}{v_x} \tag{2.14a}$$

$$mv_x(\dot{\beta} + \omega_z) = F_{y,f} + F_{y,r} \tag{2.14b}$$

The equations can be rearranged and assembled in a state space model according to equation (2.15). The relation between lateral forces and cornering stiffness C_α will be described in section 2.2.

$$\begin{bmatrix} \dot{\beta} \\ \dot{\omega}_z \end{bmatrix} = \begin{bmatrix} \frac{-C_{\alpha,f}-C_{\alpha,r}}{mv_x} & \frac{-L_f C_{\alpha,f}+L_r C_{\alpha,r}}{mv_x^2} - 1 \\ \frac{-L_f C_{\alpha,f}+L_r C_{\alpha,r}}{I_{zz}} & \frac{-L_f^2 C_{\alpha,f}-L_r^2 C_{\alpha,r}}{I_{zz}v_x} \end{bmatrix} \begin{bmatrix} \beta \\ \omega_z \end{bmatrix} + \begin{bmatrix} \frac{C_{\alpha,f}}{mv_x} \\ \frac{L_f C_{\alpha,f}}{I_{zz}} \end{bmatrix} \delta_f \tag{2.15}$$

2.2 Tire Modeling

The tires are the connection between the actuated torques from the vehicle to the forces generated on the surface, which produces the desired motion. Therefore, the dynamics of the tires play a major role in modeling the behavior of the vehicle.

2.2.1 Tire Slip

An important concept when understanding tire dynamics is tire slip. In a longitudinal sense, the slip is expressed as a ratio between the circumferential tire speed and the wheel hub speed. This describes how much the tire is sliding on the surface, and the mathematical expression for this can be seen in equation (2.16). Here, R is the radius of the wheel, ω is the angular velocity and v_{wx} is the longitudinal speed of the of the wheel. Depending on if the vehicle is accelerating or braking, different definitions of the slip are used. The denominator will be $R\omega$ when accelerating, and v_{wx} when braking.

$$s_x = \frac{R\omega - v_{wx}}{\max\{R\omega, v_{wx}\}} \tag{2.16}$$

The lateral tire slip can be described as the relation between tire speed and the lateral wheel hub speed. This phenomena occurs when changing the steering angle to alter the heading, for example when performing cornering. The expression for lateral slip is shown in equation (2.17), where v_{wy} is the lateral wheel hub speed.

$$s_y = \frac{v_{wy}}{|R\omega|} \tag{2.17}$$

The lateral slip is also associated with a slip angle α, which describes the angular difference between the longitudinal direction of the tire and the direction the tire is traveling, which is explained in equation (2.18).

$$\alpha = \frac{v_{wy}}{|v_{wx}|} \tag{2.18}$$

The concept of lateral tire slip is illustrated in figure 2.2, where δ is the steering angle and α is the tire slip angle.

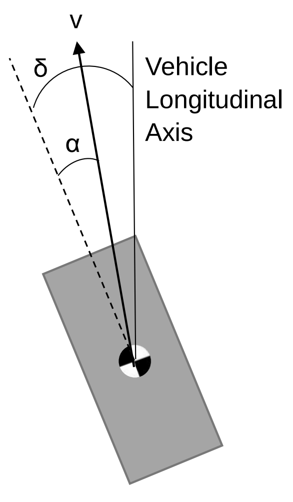

Figure 2.2: Illustration of lateral tire slip, with δ representing the steering angle and α, the tire slip angle.

Since realistic driving scenarios often include both a longitudinal and lateral velocity, a combined slip can be used to explain the slip behavior in these scenarios. Here, the resulting force on the tire is lower bounded by the resulting friction force. This can be formulated according to equation (2.19).

$$F_{wx}^2 + F_{wy}^2 \leq (F_{wz}\mu)^2 \tag{2.19}$$

2.2.2 Tire Force Modeling

This section presents different models of varying complexity for the longitudinal and lateral forces generated by the wheels.

2.2.2.1 Linear Models

The forces acting on the wheels are described by non-linear functions but can be approximated as linear functions for small slip values which can be seen in figure 2.3. The forces in the linear region can be described according to equation (2.20) where C_x is the longitudinal tire stiffness and C_α is the cornering stiffness.

$$F_{wx} = C_x s_x \tag{2.20a}$$

$$F_{wy} = -C_\alpha \alpha \tag{2.20b}$$

The dynamics of the wheel can be described according to equation (2.21) where T is the torque applied at the hub of the wheel and J_w is the inertia of the wheel.

$$J_w \dot{\omega}_w = T - F_{xw} R \tag{2.21}$$

If $\dot{\omega}_w = 0$, the tire force can be expressed using the force-torque relationship according to equation (2.22).

$$F_{wx} = \frac{T}{R} \tag{2.22}$$

These tire force relationships are useful for control techniques and will therefore be further explored in chapter 4.

2.2.2.2 Magic Formula Tire Model

A widely adopted model is the Magic Formula tire model which was developed by Hans B. Pacejka [9]. This is a semi-empirical model and uses four input parameters, B, C, D and E to provide a function for the force as a function of tire slip. The general expression for this model can be seen in equation (2.23), where x denotes the slip parameter of interest.

$$F(x) = D \sin(\arctan(Bx - E(Bx - \arctan(Bx)))) \tag{2.23}$$

In figure 2.3, the Magic Formula tire model is illustrated for the longitudinal case, in different road conditions. The four parameters are changed in each case to model the different behaviors of the different road conditions. Here, the y-axis shows the longitudinal force normalized with the normal force, while the x-axis shows the longitudinal tire slip.

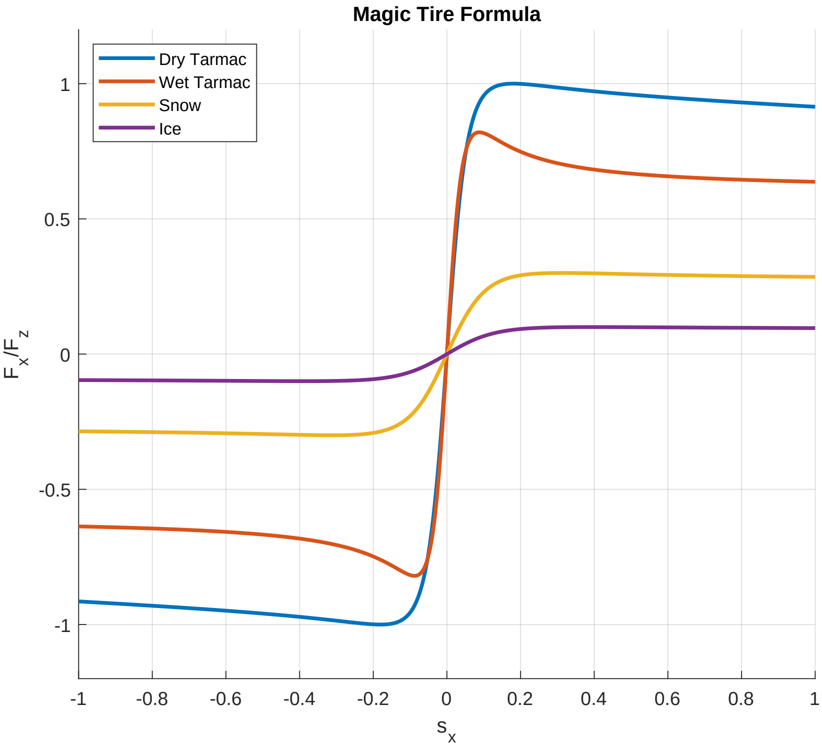

Figure 2.3: Magic Formula tire model for different road conditions.

It can be observed that the road condition, in other words the coefficient of friction μ, strongly affects the relation between tire slip and force. This is a useful insight when trying to implement slip control to achieve smoother accelerations on icy roads, for instance.

2.3 Electric Motors

In a configuration such as the proposed distributed powertrain in this thesis, different types of motors can be used on each axle. In this way, the axles can be equipped with motors that are optimal for the functionality and performance requirements of each respective axle.

2.3.1 PMSM - Permanent Magnet Synchronous Motors

Permanent magnet synchronous motors are characterized by their high power density and high efficiency [10] which makes them a suitable fit for the cruise axle, where the power request will be relatively stable and continuous. These types of motors often have high torque capabilities as well, which is convenient for the cruise axle. Since this axle is designed to operate within the entire speed range of the vehicle, it needs to have a lower gear ratio. Thus, this places constraints on the motor to have relatively high torque capabilities in order to be able to handle lower velocities, which is exactly what the PMSM can provide.

2.3.2 IM - Induction Motors

Induction motors are another type of electric motors used for electric propulsion, and can be characterized by their reliability and robustness [10]. In [1] it was suggested adding a clutch to the startability axle to disconnect the induction motors when the axle is not in use. Thus, the losses from the motors could be lowered. This makes these types of motors suitable for the startability axle. Since this axle is to be used only when additional power is needed, it will be efficient from an energy perspective to have motors with lower losses when they are not actively used.

2.3.3 Modeling of Electric Motors

The modeling of the electric motors in this thesis is based on a first order system, which has been used in previous works such as [11] and [12]. Thus, if $T_{EM,req}$ denotes the requested torque from the electric motor, it will be delayed by a time constant τ_{EM} due to the actuator dynamics. The actual torque from the motor, $T_{EM,act}$, can therefore be described as shown in equation (2.24).

$$T_{EM,act}(s) = \frac{T_{EM,req}}{\tau_{EM} s + 1} \tag{2.24}$$

Furthermore, the operating capabilities of electric motors are also described by their respective motor map. The simplified motor maps used for modeling in this analysis can be seen below in figure 2.4 and 2.5. These motor maps are based on the characteristics of the predefined motors from Volvo mentioned in section 1.3.

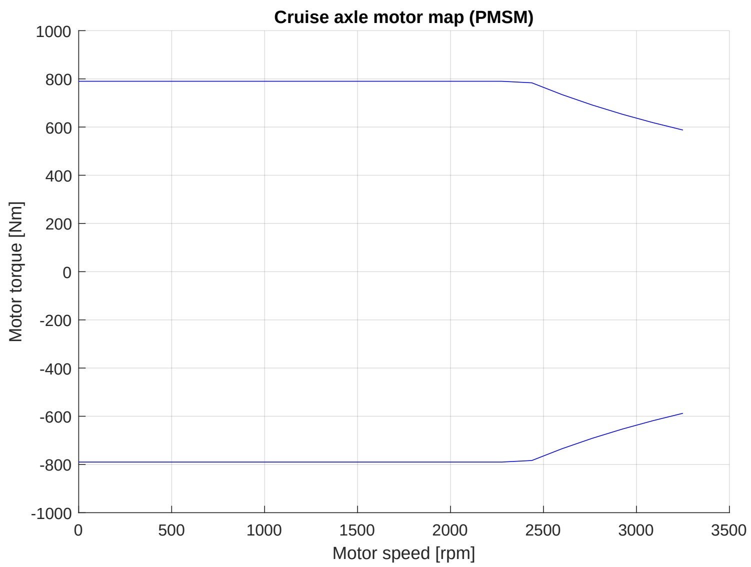

Figure 2.4: Illustration of the motor map used for the motors on the cruise axle.

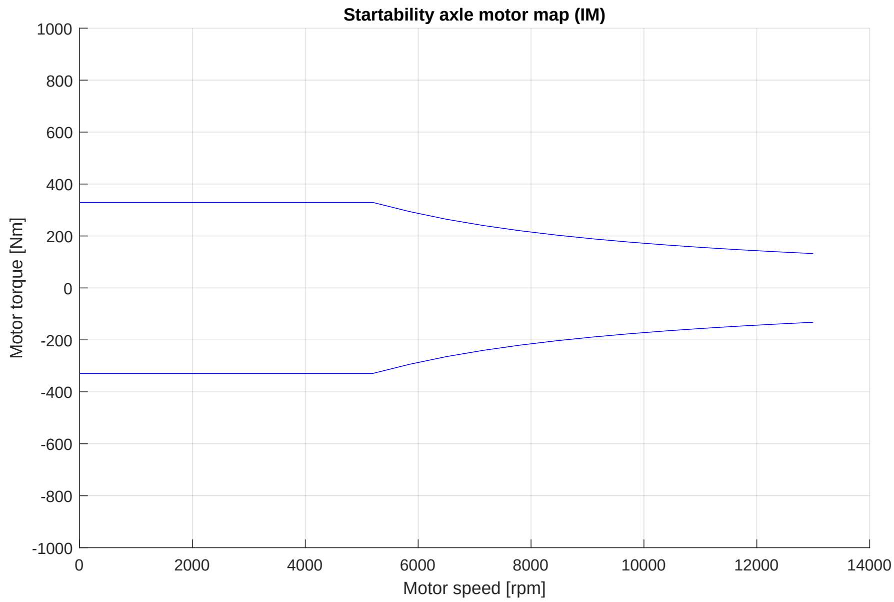

Figure 2.5: Illustration of the motor map used for the motors on the startability axle.

2.4 Brake Systems

The brakes are modeled as a first order system, where the actual torque requested from the brakes are delayed by a time constant τ_B. Let $T_{B,req}$ denote the requested brake torque on a wheel. The actual torque delivered, $T_{B,act}$, can thus be described by equation (2.25).

$$T_{B,act}(s) = \frac{T_{B,req}}{\tau_B s + 1} \tag{2.25}$$

The limits of the brakes are based on the assumption that the maximum retardation capability of the truck is -0.6g, with the total braking torque split equally between the four wheels.

2.5 Steering System

In order to control the direction in which the vehicle is traveling, a steering system is needed. The steering system is an important aspect when trying to implement steer by propulsion. Similar work has been done in a previous work which investigated steer by braking, and thus, the modeling in this section has been inspired by [13].

Electric power steering is the standard steering system used today. This allows for a smoother and easier driving experience with the help of the torque added from an electric motor, which turns the wheels to the desired steering angle. However, with steer by propulsion the idea is to generate a difference in torque on the front electric machines in order to achieve this steering angle. In some driving scenarios, this difference in torque can create what is known as torque steer, which is an unwanted effect that causes the vehicle to change steering angle without the driver requesting it. With the help of the fast response from the electric machines, steer by propulsion seeks to exploit this phenomena by deliberately creating a difference in torque on each front wheel. To describe this, equation (2.26) shows how the difference in force on each front wheel affects the total moment about the front axle, M_{steer}.

$$M_{steer} = (F_{wx,2} - F_{wx,1})r_s \tag{2.26}$$

Here, r_s is a parameter known as the scrub radius. On the steering axle, a kingpin bolt is mounted. This is often mounted at an angle which will affect the characteristics of the steering system. The line that passes through the kingpin bolt is called the kingpin axis. Thus, the scrub radius is defined as the distance between where the kingpin axis meets the road, and where the centerline of the tire meets the road. An illustration of this can be seen in figure 2.6, where the kingpin bolt is highlighted in orange.

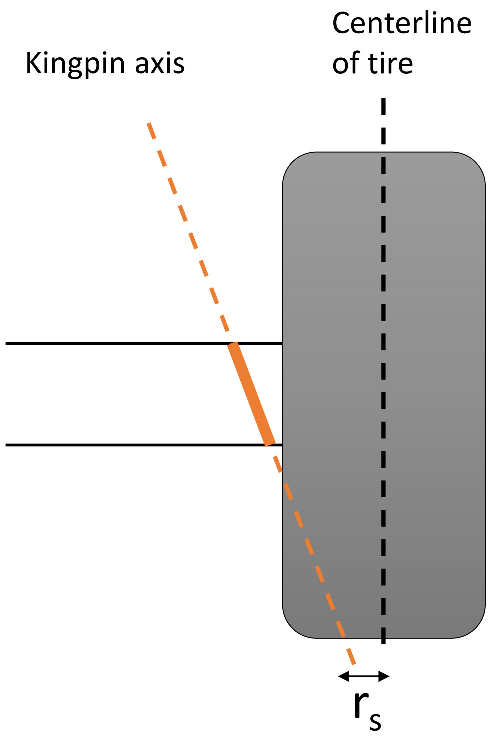

Figure 2.6: Illustration of the scrub radius r_s.

Lateral forces acting on the tire will cause an aligning moment that will counteract the turning of the wheels as explained in [13] and [14]. During driving, stress on the tires will cause deformation of the rubber and generate these forces. The resulting lateral force from the deformed contact patch acts at a point, which is located at a distance from the center of the tire defined as pneumatic trail, t_p. The wheel is also mounted with a caster angle τ that defines what is known as mechanical trail,

t_m. A moment about the kingpin axis is therefore generated according to equation (2.27).

$$M_y = (t_m + t_p)(F_{wy,1} + F_{wy,2}) \tag{2.27}$$

In [14], a vehicle using differential braking was analyzed. The scrub radius effect was taken into account in the modeling. The steering system was modeled as a second order differential equation, and a similar model was used in [13] as well. An adaption for the vehicle model in this thesis can be seen in equation (2.28) where other moments on the steering axle have been lumped into $M_{resistive}$. Here, I_s is the inertia of the front axle and b_s a damping factor.

$$I_s\ddot{\delta}_f + b_s\dot{\delta}_f = M_{steer} - M_y - M_{resistive} \tag{2.28}$$

3 Concept Vehicle Analysis

In this chapter, a vehicle with the proposed powertrain concept is analyzed. This should not be regarded as the only possible powertrain configuration, however. Instead, the purpose here is to briefly explain and illustrate the performance capabilities, as well as the possible control strategies of the cruise and startability concept.

3.1 Performance Analysis & Powertrain Sizing

To conduct an analysis of the vehicle performance and requirements, the vehicle model needs to be defined. In table 3.1, the vehicle parameters and performance requirements are presented for a simple vehicle model based on the proposed powertrain.

Vehicle parameter / performance requirement	Value
Gross combined weight m [kg]	35000
Wheel radius R [m]	0.506
Air density ρ_{air} [kg/m^3]	1.2
Gravity constant g [m/s^2]	9.81
Air drag coefficient c_d [-]	0.59
Rolling resistance coefficient c_r [-]	0.005
Frontal area A_f [m^2]	10
Cruise velocity [km/h]	85
Cruise axle maximum/minimum road gradient [%]	± 2
Startability axle maximum road gradient [%]	10
Cruise axle gear ratio [-]	4.5
Startability axle gear ratio [-]	26

Table 3.1: Table presenting vehicle parameters and performance requirements.

The traction force needed to propel the vehicle longitudinally is counteracted by mainly three resistive forces: air resistance, rolling resistance and road gradients as mentioned in section 2.1. In figure 3.1, a traction force diagram showing the resistive forces is illustrated, with dashed lines representing the traction force needed at different road gradients.

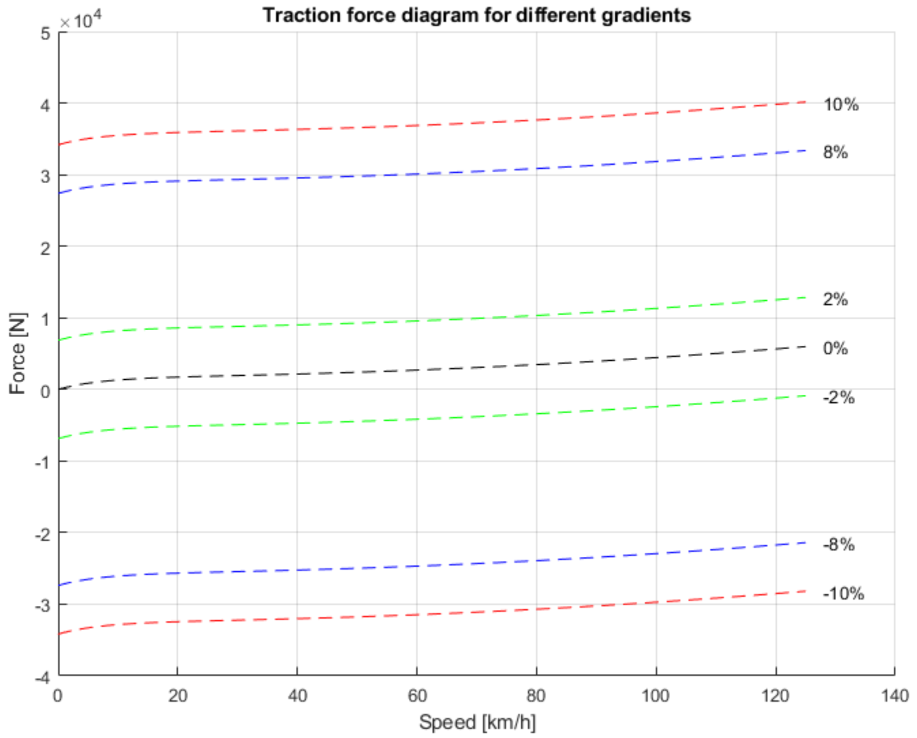

Figure 3.1: Traction force diagram for the resistive forces. The dashed lines indicate the required traction force for different road gradients.

With the provided reference motors from Volvo and the gear ratios presented previously, the sizing of the powertrain can be commenced. First, the performance requirements of the cruise axle are analyzed to find the appropriate motor characteristics and capabilities. These results can then be used for analyzing the startability axle, which is to be used in combination with the cruise axle when additional power is needed. With the provided reference motors, simple motor maps can be created in MATLAB which are then used to illustrate the force-speed characteristics of the axles. Figure 3.2 illustrates the traction force diagram for each axle and combined axles, plotted together with the performance requirements. This shows that the proposed powertrain concept functions well in this application as it fulfills the desired performance requirements, both on each respective axle, as well as the combined axle requirement such as starting in the maximum road gradient.

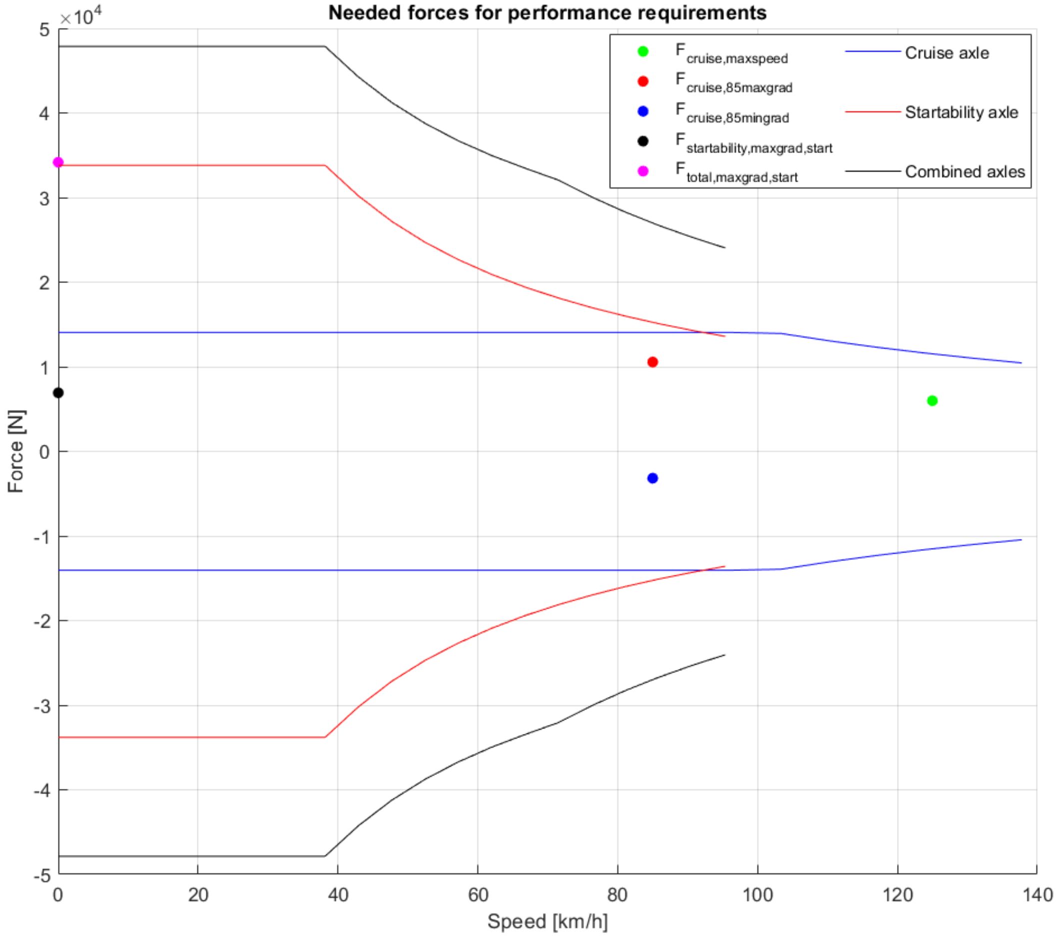

Figure 3.2: Force capabilities of the cruise axle, startability axle and combined axles illustrated together with the performance requirements specified in table 3.1. The capabilities of the axles are with gear ratios included.

To further illustrate the performance capabilities of the proposed powertrain, figure 3.3 shows the required traction forces for different road gradients plotted together with the force-speed diagram of the powertrain. This figure shows that some performance requirements could likely be increased with the proposed powertrain and reference motors, such as maximum/minimum road gradient and maximum velocity.

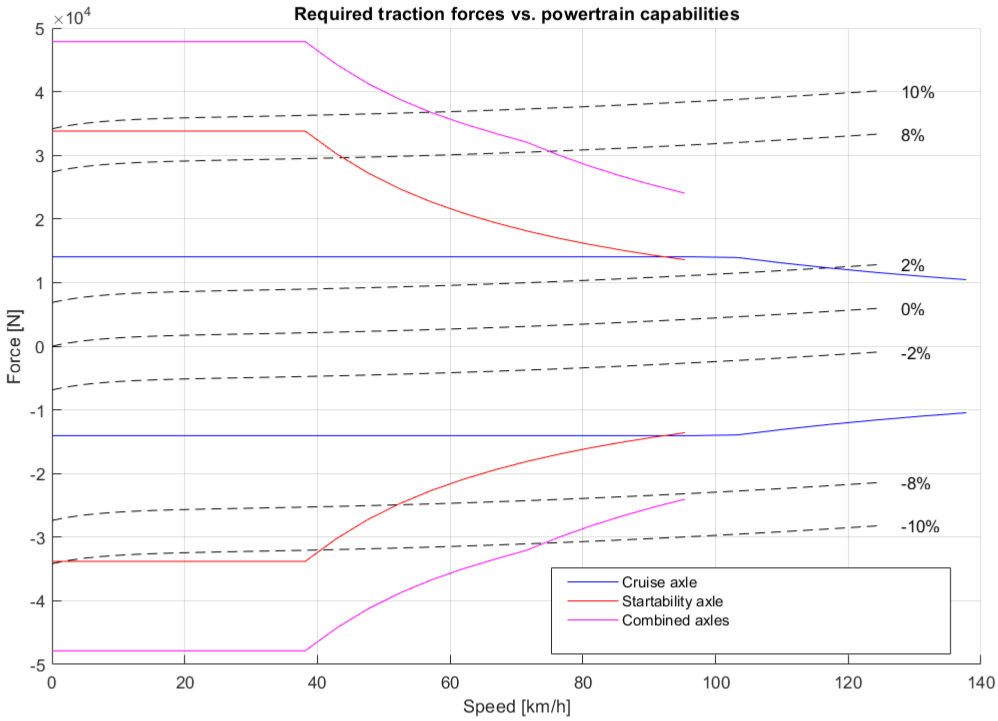

Figure 3.3: Required traction force for different road gradients illustrated together with the powertrain capabilites of the cruise axle, startability axle and combined axles.

3.2 Sensitivity Study

A minor sensitivity study is presented here to show how variations in vehicle design parameters such as roll coefficient, air drag coefficient and gears change the requirements of the powertrain. These studies are all conducted for maintaining cruise speed at 2% slope, i.e. at 85 km/h where the cruise axle handles the propulsion of the vehicle. This is the speed where the long haul vehicle travels at most time instances, and thus, it serves as a suitable reference speed for the sensitivity study.

Below, table 3.2 shows how the total power requirements on the cruise axle is affected due to changes in the roll coefficient and air drag coefficient.

c_r [-]	c_d [-]	Required cruise axle power [kW]
0.005	0.59	249
0.004	0.59	241
0.005	0.472	240
0.004	0.472	232

Table 3.2: Effects of changes in the roll and air drag coefficients on the total power requirements on the cruise axle at cruise speed in a 2% slope.

It can be observed that a 20 % reduction of the roll coefficient means the total power requirement on the cruise axle is reduced from 249 kW to 241 kW, i.e. a reduction of 3.2%. Meanwhile, a 20 % reduction of air drag coefficient means the total power requirement on the cruise axle is reduced from 249 kW to 240 kW, i.e. a reduction of 3.6%. Finally, a 20 % reduction in both parameters results in a reduction on the required power of 6.8 %. Thus, these parameters are important to keep in mind when designing an energy-efficient vehicle.

The choice of gears is a trade-off between maximum torque and maximum wheel speed. The design has to make sure that both axles can produce wheel speeds that correspond to the maximum speed of the vehicle. At the same time, the torque required for overcoming road gradients and performing accelerations needs to be considered as well. Thus, the choice of gears needs to take several factors into account, such as motor choice, performance requirements on each axle, costs, weight etc. In table 3.3, a comparison is made to see how different gear ratios on the startability axle affects the peak longitudinal force and the corresponding maximal speed the axle can generate.

Gear ratio	F_x [N]	v [km/h]
25:1	32500	99
26:1	33800	95
27:1	35100	92
28:1	36400	89

Table 3.3: The table shows the peak force that the startability axle can generate with a set of different gears as well as the corresponding maximal speed due to the motor being limited to a maximum motor speed.

3.3 Control Analysis

This section will describe the control possibilities of a distributed powertrain such as the one in the suggested configuration. Individual and fast control of each motor allows for a variety of different control strategies. These strategies could be targeted at achieving a specific goal, such as minimizing the energy consumption or increasing vehicle stability.

3.3.1 Torque Vectoring Concept

The shift to electric vehicles with new powertrain architectures has made torque vectoring a popular research topic. In comparison to combustion-based vehicles, electric vehicles can more easily be fitted with a distributed powertrain. The torque of each wheel or a set of wheels on the vehicle can be individually controlled by placing individual motors on the wheels. Electric motors also have a faster response time than combustion engines. Hence, the wheels can be controlled more accurately. Traditional vehicles are usually fitted with a combustion engine, driveshafts and differentials to distribute the torque to the wheels. Most vehicles have what is known as open differentials, which means that the torque from the engine is evenly split between the wheels. The concept of torque vectoring therefore arises from the possibility to individually control the torque of a wheel and is illustrated in figure 3.4.

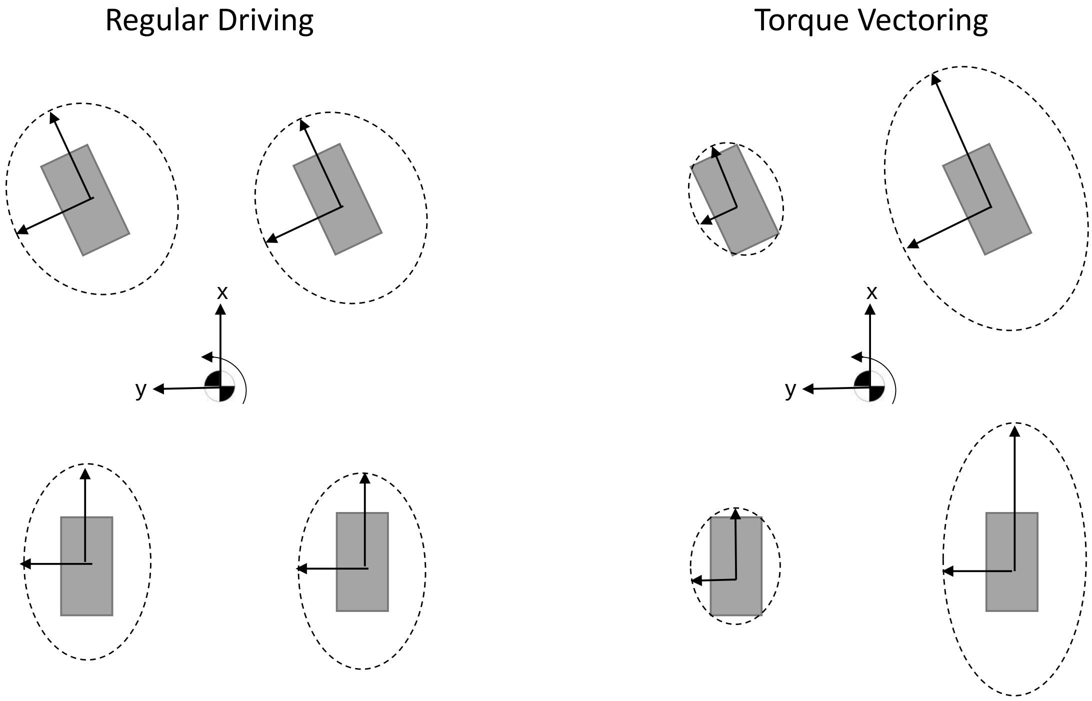

Figure 3.4: Illustration of how vehicle forces might be distributed for a regular vehicle, and how it might be distributed using torque vectoring. The arrows indicate the direction of the longitudinal and lateral force on each wheel. The ellipses indicate the magnitude of the total force on each wheel.

Torque vectoring can be achieved in multiple ways using different control strategies, where figure 3.4 is meant to illustrate the concept. In the illustration above, the vehicle is turning left and it can be seen how a regular four-wheel drive vehicle distributes the wheel torques equally. It can also be seen how a torque vectoring algorithm could distribute the torque on each wheel. When performing a left turn, a load transfer to the outer wheels will occur. Greater traction can therefore be supplied by these wheels, assuming that all wheels are driving on the same surface. Improved cornering can therefore be achieved by increasing the torques on the outer wheels.

A wide range of vehicle functions can be achieved through torque vectoring. Locking differentials is a common function that allows regular vehicles to achieve better traction when driving on roads with varying surfaces, by forcing the wheels to rotate at the same speed. By requesting torque on the side with better traction, the same function can be achieved with torque vectoring. Anti-lock braking system (ABS) is another common function to assist drivers in slippery conditions. Torque vectoring can be used to achieve the same functionality through the fast and accurate individual control of the wheels. The algorithms for torque vectoring vary in complexity, from simply scaling the torque on the outer and inner wheel depending on the steering angle, to model predictive controllers including vehicle constraints. In chapter 4, an algorithm is proposed for the concept vehicle in this thesis.

3.3.2 Steer By Propulsion Concept

In this thesis, the concept of steer by propulsion is introduced. This method uses differential torque applied from the front electric motors to turn the wheels. A similar technique was introduced in [13], but by using the brakes instead. Differential braking is also a closely related topic and has been studied in [14]. SBP can be viewed as a specific torque vectoring algorithm since different torques are being applied to the wheels, but SBP is more targeted at steering angle control. Furthermore, SBP can make use of regenerative braking in order to achieve a differential torque on the front axle. The main difference between [13] and SBP is that the front axle should propel the vehicle, as well as handling the steering requests. The concept is illustrated in figure 3.5.

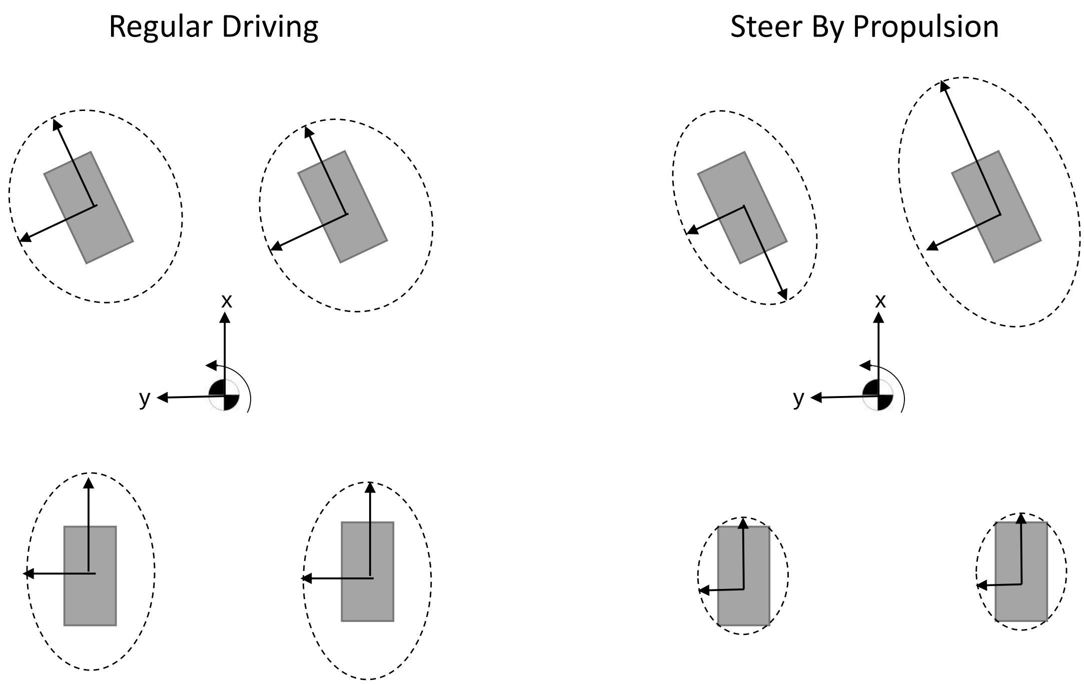

Figure 3.5: Illustration of how vehicle forces might be distributed for a regular vehicle, and how it might be distributed for a vehicle using SBP. The arrows indicate the direction of the longitudinal and lateral force on each wheel. The ellipses indicate the magnitude of the total force on each wheel.

The fundamental physics that makes steer by propulsion possible, is due to the scrub radius that was introduced earlier. A moment, M_{steer}, about the kingpin axis is needed to turn the wheels, where the scrub radius is the moment arm that generates the torque through the longitudinal force applied on the wheels. Simply applying differential torque on the wheels of the front axle does not guarantee that the wheels will turn. It is therefore important to design the wheel suspension in such way that a satisfactory positive scrub radius is achieved.

The range of steering angles that can be achieved using SBP will be different compared to regular steering. Friction forces, scrub radii and motor torques will limit how large steering angle that can be achieved using steer by propulsion. On surfaces with low friction such as ice, only smaller steering angles can be achieved due to the limiting tire forces. There is also a risk of understeering, as SBP will require significant longitudinal forces to turn the wheels.

The driving characteristics are also worth considering, since the differential torque will not only achieve the steering angle but also add yaw moment. The yaw moment achieved for a given steering angle using SBP will therefore be larger than for regular steering. The characteristics of the vehicle is changed, and might be something that needs to be considered for a driver to have a comfortable driving experience. In chapter 4, the control design is explained and a method is proposed to handle the differences in characteristics.

4

Control Design

This chapter starts with presenting an overview of the chosen control system structure. Thereafter, the subsystems of the structure are described in more detail. All control strategies are designed for the tractor. In chapter 5, a semitrailer is added for testing purposes but is not part of the controlled unit.

4.1 Control System Structure

An overview of the control system for the truck can be seen in figure 4.1. This structure is designed to fit the current Volvo software architecture. To coordinate the motion of the truck, a high level motion controller calculates a set of virtual forces **v** acting on the truck in order to achieve the desired behavior. This controller receives reference entities **ref** from a reference generator based on the input from the driver, i.e. the desired acceleration and steering angle. Since the truck is over-actuated and the control system should satisfy a multi-objective control problem, this poses a challenge of deciding the optimal use of the available actuators in the control input **u**. Control allocation, which is formulated as an optimization problem that aims to minimize an objective function while satisfying a set of constraints, is an effective approach to solve the problem and is thus applied. It is difficult to estimate different parameters and other constraints of the motion of the vehicle, which is why the control system is designed with wheel controllers. These controllers handle constraints such as torque limits and speed limits internally, making sure that the vehicle can operate safely and efficiently. Each respective wheel controller outputs a torque T for each respective motor.

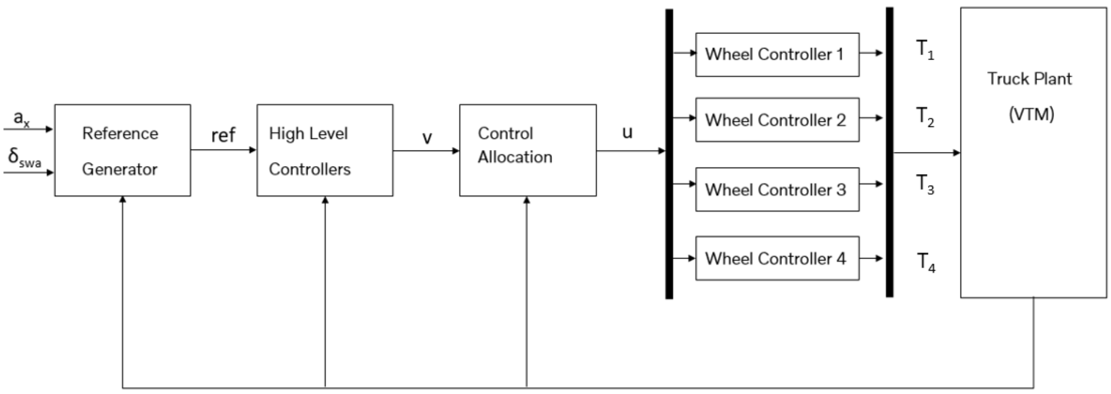

Figure 4.1: A simple visualization of the control system architecture.

4.2 Path Follower

A Stanley controller [15] was implemented in the thesis and an illustration of the geometry used to derive the control law can be seen in figure 4.2. The controller tries to eliminate the heading error which is the difference between the heading of the path, θ_t, and the heading of the vehicle θ_c. It also aims at eliminating the cross track error e which is the distance between the front axle of the vehicle and the closest point on the path.

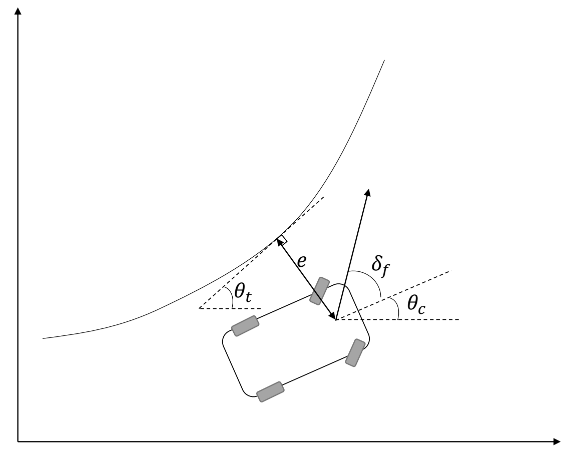

Figure 4.2: Illustration of geometry used for the implementation of the Stanley controller.

The elimination of the heading error can be defined according to equation (4.1).

$$\delta_1 = \theta_t - \theta_c \tag{4.1}$$

The steering angle to correct for the cross track error can be formulated according to equation (4.2) where k is the gain, which is a design parameter.

$$\delta_2 = \tan(\frac{ke}{v_x})^{-1} \tag{4.2}$$

The steering angle is finally defined according to equation (4.3).

$$\delta_f = \begin{cases} \delta_f^{max}, & if \;\; \delta_1 + \delta_2 \geq \delta_f^{max} \\ \delta_f^{min}, & else\; if \;\; \delta_1 + \delta_2 \leq \delta_f^{min} \\ \delta_1 + \delta_2, & else \end{cases} \tag{4.3}$$

4.3 Control Allocation

When dealing with over-actuated systems, control allocation is an appropriate method to use. Here, the approach is to formulate the allocation of total control action among several actuators in an over-actuated system, as an optimization problem. This section provides the general formulation, how actuator limits are defined and how the weights are set in the optimization problem. The available actuators in this study are limited to the electric motors, service brakes and a power steering system. The specific formulation for this thesis is presented in the next section.

4.3.1 General Formulation

The mathematical formulation of a control allocator is to solve an underdetermined and often constrained system of equations [16]. In the case of over-actuated systems, there exists multiple potential ways of achieving the desired vehicle motion with the available actuators in the control input vector $\mathbf{u} \in \mathbb{R}^m$. Thus, another formulation is to define the virtual control input $\mathbf{v} \in \mathbb{R}^n$, where $m > n$. This vector describes the desired output entities such as longitudinal force, lateral force and yaw moment. The mapping between $\mathbf{u}$ and $\mathbf{v}$ is done through the so called control effectiveness matrix, B, which in this case is assumed to be linear. The B matrix describes how the actuators relate to the desired output entities in $\mathbf{v}$. This relation is described in equation (4.4).

$$\dot{x} = f(x) + \underbrace{B\mathbf{u}}_{\mathbf{v}} \tag{4.4}$$

With this formulation in hand, the optimization problem can be constructed to solve for the optimal control input $\mathbf{u}$. This optimization consists of two objectives. The first objective is to use the prioritized actuators as often as possible. Thereafter, the second objective is to construct a control input $\mathbf{u}$ such that the difference between $B\mathbf{u}$ and the virtual control input $\mathbf{v}$ is minimized. To combine these objectives, the weighted least squares method is used to solve the problem. The complete optimization problem is shown in equation (4.5).

$$\mathbf{u} = \underset{\underline{\mathbf{u}} \leq \mathbf{u} \leq \bar{\mathbf{u}}}{\arg\min} ||W_u(\mathbf{u} - \mathbf{u_{des}})||^2 + \gamma ||W_v(B\mathbf{u} - \mathbf{v})||^2 \tag{4.5}$$

Here, the optimization is constrained to the actuator limits $\underline{\mathbf{u}}$ and $\bar{\mathbf{u}}$. The weighting matrix W_u allows for prioritizing of different actuators to be used. Similarly, W_v allows for prioritizing of desired output entities. $\mathbf{u_{des}}$ contains the desired actuator usage, which will be explained in more detail in section 4.3.5. Finally, the factor γ is used to prioritize between the two objectives of the optimization.

4.3.2 QP Formulation

The general control allocation problem can be solved using different optimization algorithms and a variety of these were investigated in [17] and [18]. To use available solvers, the problem can be formulated as a QP optimization problem. The standard form is expressed in equation (4.6).

$$
\begin{aligned}
\min_{u} \quad & \frac{1}{2}u^T H u + f^T u \\
\text{s.t.} \quad & A_{eq} u = b_{eq}, \\
& A_{in} u \leq b_{in}, \\
& \underline{u} \leq u \leq \bar{u}
\end{aligned} \tag{4.6}
$$

Through algebraic manipulation of the general control allocation formulation in equation (4.5), it can be found that the matrices H and f can be expressed as in equation (4.7).

$$
H = 2(W_u^T W_u + \gamma B^T W_v^T W_v B) \tag{4.7a}
$$

$$
f^T = -2(u_d^T W_u^T W_u + \gamma v^T W_v^T W_v B) \tag{4.7b}
$$

4.3.3 Actuator Dynamics Constraint

The dynamics of the actuators can be included in to the control allocation formulation by using models of the actuators. It can be noted that there are many situations where the dynamics does not need to be considered. However, to properly reflect the controlled system, dynamic models are used to limit the rate of change for actuators. Hence, the control allocator won't be able to request unreasonable actions by the actuators. Electric motors and brakes are modeled as first order filters and the dynamics can be written according to equation (4.8) where τ is the time constant of the system and T^{req} is the requested actuator level.

$$
\tau \dot{T} = T^{req} - T \tag{4.8}
$$

The control allocator is a discrete time controller which makes it possible to describe the derivative as change of the state. An approximation of the derivative can be found by using the Euler forward method according to equation (4.9) where T_s is the sampling time of the controller.

$$
\dot{T} = \frac{T(k+1) - T(k)}{T_s} = \frac{\Delta T}{T_s} \tag{4.9}
$$

Combing equation (4.8) and (4.9) gives the maximum and minimum rate of change for the given sampling time of the controller. The rates can be calculated according to equation (4.10a) and (4.10b), where T_{max} and T_{min} are the current operating capabilities of the actuator.

$$
\Delta T_{max} = \frac{T_s}{\tau}(T_{max} - T) \tag{4.10a}
$$

$$
\Delta T_{min} = \frac{T_s}{\tau}(T_{min} - T) \tag{4.10b}
$$

4.3.4 Tire Force Constraint

In order to take the limitations of the tires into account, the CA formulation has to include constraints on the allocated torque with regards to the limitations on the tires. A technique known as tire fusion [11] has been used in previous works to add this dynamic constraint to the CA formulation. The tire fusion compares the current capabilities of the tires to the current capabilities of the motors and brakes. If the tire capabilities are lower than the motor capabilities, the updated limit is set according to the tire limits. Here, the maximum capability of a tire is estimated according to equation (4.11). As can be observed, the maximum capability is defined as a percentage of the peak friction force of the tire, where the factor ξ defines this percentage. In this way, some of the tire capabilities can be used for lateral motion as well.

$$F_{x,max} = F_z \mu \cdot \xi \tag{4.11}$$

It should also be noted that this technique favors the use of the electric motors to drive in an energy-efficient manner. Thus, if the electric motor output is limited due to actuator limitations, the remaining torque is delivered by the brakes. The tire fusion concept can be described by the set of equations in (4.12) - (4.15), where the upper and lower limits on the motors and brakes are calculated. Here, the set of equations uses a similar notation as in [11].

$$T_{EM}^{upper} = \begin{cases} F_{x,max}R, & \text{if } F_{x,max}R \leq T_{EM}^{upper} \\ T_{EM}^{upper}, & \text{otherwise} \end{cases} \tag{4.12}$$

$$T_{EM}^{lower} = \begin{cases} -F_{x,max}R, & \text{if } -F_{x,max}R \geq T_{EM}^{lower} \\ T_{EM}^{lower}, & \text{otherwise} \end{cases} \tag{4.13}$$

$$T_{B}^{upper} = 0 \tag{4.14}$$

$$T_{B}^{lower} = \begin{cases} 0, & \text{if } -F_{x,max}R \geq T_{EM}^{lower} \\ -F_{x,max}R - T_{EM}^{lower}, & \text{else if } (T_{EM}^{lower} + T_{B}^{lower}) \leq -F_{x,max}R \\ T_{B}^{lower}, & \text{otherwise} \end{cases} \tag{4.15}$$

4.3.5 Desired Actuator Usage

The desired usage of the actuators can be specified in the $\mathbf{u_{des}}$ vector. The weighted least squares formulation will try to solve the multi-objective optimization problem in the best way in order to both satisfy the virtual forces and achieving the desired motion, as well as prioritizing the usage of different actuators. An energy management system could provide how the actuators should be used in order to minimize the total energy consumption. If the desired usage is specified as zeros, then the interpretation based on the weighting would be how expensive it would be to use an actuator. Larger weights make it expensive to use that specific actuator, while a low weight will favor the usage of that actuator. If instead specific values are given in $\mathbf{u_{des}}$, the interpretation will be that with large weights, it is expensive to deviate from the desired values. It is favorable to use the interpretation of how expensive it is to use an actuator. This makes it possible to set the weights of each actuator to achieve the desired behavior of each respective axle.

4.3.6 Dynamic Weighting

Since different driving scenarios require different performances and use of actuators, the weighting matrices W_u and W_v can be dynamically changed throughout continuous driving to adapt to the situation optimally. Dynamic weighting has been used in previous works [7][17] with promising results and was therefore deemed a suitable addition to the CA formulation. Depending on the driving conditions it might be favorable to prioritize certain global forces. An example of such a case, as suggested in [17], is when driving on high-μ surfaces. Here, rollover is at larger risk than yaw instability. Therefore it is better to prioritize longitudinal forces over yaw moment. On low-μ, yaw instability is at higher risk and should therefore be prioritized.

The following dynamic weights are based on the concept about actuator usage previously presented, i.e lower weight prioritizes the usage of that actuator. A concept that has been used in several works at Volvo and was introduced in [17] was to scale the weight of each wheel actuator, that is the motors and brakes, with the inverse square root of the normal force on each respective wheel according to equation (4.16). Using this approach allows to efficiently upper bound how a wheel actuator can be used, since a higher normal load usually provides the possibility of more traction. This is however not true in the case of split-μ. The factor $\beta^{i,j}$ remains to be defined and is also dynamically changed depending on the situation. The square root in the first factor is simply a scaling done in the previous work mentioned above, used in combination with other factors. Therefore, the same factor is chosen here as a starting point, and $\beta^{i,j}$ is chosen to achieve the desired behavior in combination with this factor.

$$W_u^{i,j} = \frac{1}{\sqrt{F_{z,i}}}\beta^{i,j}, \quad i \in \{LF, RF, LR, RR\}, \quad j \in \{B, EM\} \tag{4.16}$$

The vehicle concept uses the front axle as cruise axle and the rear axle as a startability or power axle and the dynamic weighting can therefore realize the concept. In most cases, $\beta^{i,j}$ will be low for the front motors since they are highly efficient and have higher losses when not used. The weighting for the rear motors are normally higher but will decrease in case of acceleration or driving uphill. The brakes will usually have the highest weight, since it is undesirable to use them due to energy losses when the motion requests are in the operating range of the electrical motors. The weight of the steering actuator can be tuned depending on the amount of torque vectoring that is desired.

4.4 Torque Vectoring

The structure of the control system is based on the possibility to assist a manual driver as well as an autonomous driving (AD) system. Two of the proposed control schemes will mainly be intended for applications in an AD system. However, it could also function in a steer-by-wire system. An interface with acceleration request, a_x, and steering angle request, δ_f, is therefore the communication between the driver/AD system and the motion controller. There are several layers of the control system as shown in figure 4.1. All the layers for two different torque vectoring algorithms will be explained in this section.

The reference generator provides references for the longitudinal speed v_x^{ref}, steering angle, δ_f^{ref}, and yaw rate, ω_z^{ref}. These references are then fed to high level controllers. The reference generation is based on the fact that a driver expects a linear behavior of the vehicle and the same assumption is made for an AD system since the behavior is more predictable in the linear region of operation.

So far, control allocation has been explained in more general terms and in this chapter the specific implementation will be proposed. In the first approach, control allocation is used to distribute the torques and steer angle, while in the second approach the allocation of the power steering is locked. The control allocation problem and the chosen high level motion controller will be presented. Since the vehicle is equipped with four individual motors, four mechanical brakes and the front axle power steering, the control vector is defined according to equation (4.17) in both cases.

$$\mathbf{u} = [T_{b,1} \;\; T_{b,2} \;\; T_{b,3} \;\; T_{b,4} \;\; T_{EM,1} \;\; T_{EM,2} \;\; T_{EM,3} \;\; T_{EM,4} \;\; \delta_f]^T \tag{4.17}$$

The control effectiveness matrix, B, can be defined in multiple ways depending on the assumptions made in the model. In this thesis, a linear control effectiveness matrix is desired. One possible solution would be to use the common control theory approach, and linearize $\mathbf{v}$ around an operating point using a Taylor series. Another possible approach, as suggested in previous works [7], is to assume small steering angles, no body slip and that $F_{x,i} = T_i/R$. These assumptions are made in both approaches below. The following parameters are used to define B: G_{crs} denotes the gear ratio on the cruise axle, G_{str} the gear ratio on the startability axle, C_α the front axle cornering stiffness, and r_s the scrub radius on the front axle. The equations of motion from the previous chapter are repeated and presented in a similar form to equation (4.4). The mentioned assumptions will make $\mathbf{v}$ linear in equation (4.18).

$$\underbrace{\begin{bmatrix} m\dot{v}_x \\ m\dot{v}_y \\ I_{zz}\dot{\omega}_z \end{bmatrix}}_{\dot{x}} = \underbrace{\begin{bmatrix} -mv_y\omega_z \\ mv_x\omega_z \\ \sum_i M_{z,i} \end{bmatrix}}_{f(x)} + \underbrace{\begin{bmatrix} \sum_i F_{x,i} \\ \sum_i F_{y,i} \\ \sum_i M_{z,i} \end{bmatrix}}_{\mathbf{v}} \tag{4.18}$$

4.4.1 Torque Distribution Using Control Allocation

This section describes how three virtual forces, F_x, F_y and M_z, can be used to design a torque vectoring algorithm with the use of control allocation.

4.4.1.1 Motion Controller

This control system functions for both an AD system and a manual driver. To be able to control the longitudinal motion of the vehicle, a speed reference is needed. The speed reference generation is expressed according to equation (4.19) as suggested in [19], where the initial speed of the vehicle is changed according to the acceleration input at each sample time T_s of the controller. This reference is used since the driver will expect a linear behavior of the vehicle.

$$v_x^{ref} = v_{x0} + \sum_{i=0}^{t/T_s} T_s a_{x,i} \tag{4.19}$$

The reference yaw rate can be generated in multiple ways. In this thesis, it will be set as proposed in [20]. If the curvature of the road is κ then the desired yaw rate can be expressed according to equation (4.20).

$$\omega_z = \kappa v_x \tag{4.20}$$

The steering characteristics of the vehicle will be used to relate the steering angle to the yaw rate. From the equations of the single track model used in [20], under steady-state conditions, an expression that relates steering angle to curvature can be defined according to equation (4.21).

$$\kappa = \frac{\delta_f}{L_f + L_r + mK_u v_x^2} \tag{4.21}$$

The variable K_u in equation (4.22) is defined as the understeer gradient and defines the steering characteristics of a vehicle. If $K_u < 0$ the vehicle is oversteered, if $K_u = 0$ it is neutral-steered and if $K_u > 0$, it is understeered and characterizes how large steering angle that needs to be applied to follow a certain curvature.

$$K_u = \frac{C_{\alpha,r}L_r - C_{\alpha,f}L_f}{C_{\alpha,r}C_{\alpha,f}(L_f + L_r)} \tag{4.22}$$

The desired yaw rate can finally be expressed according to equation (4.23).

$$\omega_z^{ref} = \frac{v_x}{L_f + L_r + mK_u v_x^2}\delta_f \tag{4.23}$$

A combination of proportional integral (PI) controllers and feedforward controllers are implemented to achieve the requested speed, lateral forces and yaw moment. Here, the reference velocity generated in equation (4.19) is compared to the current estimated vehicle velocity to generate the longitudinal force F_x. This can be expressed as in equation (4.24), where $F_x[k]$ is the output from the PI controller at time k, K_{p,F_x} the proportional gain, K_{i,F_x} the integral gain and $\Delta v_x[k]$ the difference between the current estimated vehicle speed and the current reference speed.

$$F_x[k] = K_{p,F_x}\Delta v_x[k] + K_{i,F_x}T_s\sum_{i=0}^{k}\Delta v_x[i] \tag{4.24}$$

The lateral forces will be generated with a feedforward controller according to equation (4.25). No side slip is assumed here.

$$F_y[k] = 2C_{\alpha,f}\delta_f[k] \tag{4.25}$$

The yaw rate controller is composed of a feedback loop and a feedforward controller as shown in equation (4.26).

$$M_z[k] = \underbrace{2C_{\alpha,f}L_f\delta_f[k]}_{M_{z,feedforward}} + \underbrace{K_{p,M_z}\Delta\omega_z[k] + K_{i,M_z}T_s\sum_{i=0}^{k}\Delta\omega_z[i]}_{M_{z,feedback}} \tag{4.26}$$

4.4.1.2 Control Allocation Formulation

In the proposed torque vectoring algorithm, the steering system can be complemented by the electrical motors by using the moment that the differential forces on the front wheels generate. The virtual forces in equation (4.27) are generated through the combination of feedforward and feedback controllers, and the actuator usage is distributed using control allocation. The first method of torque vectoring that was chosen included controlling the yaw moment, lateral forces and longitudinal forces. The virtual forces for the control allocation in this method are limited according to equation (4.27). The motion control of the proposed torque vectoring algorithm is partly inspired from the thesis [20]. The thesis however, did not consider lateral forces or a control allocator to distribute the forces.

$$\mathbf{v} = \begin{bmatrix} \mathbf{F}_x \\ \mathbf{F}_y \\ \mathbf{M}_z \end{bmatrix} \tag{4.27}$$

The control effectiveness matrix is defined according to equation (4.28).

$$B = \begin{bmatrix} \frac{1}{R} & \frac{1}{R} & \frac{1}{R} & \frac{1}{R} & \frac{G_{crs}}{R} & \frac{G_{crs}}{R} & \frac{G_{str}}{R} & \frac{G_{str}}{R} & 0 \\ 0 & 0 & 0 & 0 & 0 & 0 & 0 & 0 & 2C_{\alpha,f} \\ \frac{-T_f}{2R} & \frac{T_f}{2R} & \frac{-T_r}{2R} & \frac{T_r}{2R} & \frac{-T_fG_{crs}}{2R} & \frac{T_fG_{crs}}{2R} & \frac{-T_rG_{str}}{2R} & \frac{T_rG_{str}}{2R} & 2L_fC_{\alpha,f} \end{bmatrix} \tag{4.28}$$

The requested yaw moment can be generated through the different combinations of steering actuators, electrical motors and brakes. Depending on the weighting of the actuators and virtual forces, different characteristics can be achieved. By setting low weight on the front motors, medium weight on the steering actuator and high weight on the back motors and brakes the CA will prioritize to use the front motors. This approach will hence result in the motors assisting the steering actuator and contributing with yaw moment. The added yaw moment will lead to yaw acceleration and the desired yaw rate can hence be achieved faster. The performance of this control strategy proved to be rather good. However, the main purpose of this report is to investigate steer by propulsion and no results of this torque vectoring method will be shown.

4.4.2 Steer By Propulsion

One of the main objectives of this thesis is the implementation of SBP and this section will describe the different methods. The virtual forces that are controlled in this scheme are F_x, F_y, M_z and M_{steer}. Using independent control of yaw moment according to equation (4.26) can result in an oscillating and noisy behavior in some driving scenarios. This is because the motion requests M_z and M_{steer} would be considered as independent of each other, but there is a connection between M_z and M_{steer}.

The reference yaw rate is based on regular driving but SBP can change the steering characteristics as described earlier in section 3.3.2. The connection between the motion request of M_z and M_{steer} can be derived by returning to the equations of motion. The yaw moment of the vehicle is described according to equation (4.29) with the simplifications mentioned in section 4.4. The yaw moment is divided into three parts. M_{zf} is the yaw moment achieved from the longitudinal forces on the front axle. Similarly, M_{zr} is the yaw moment achieved from the longitudinal forces on the rear axle. Finally, $M_{z\delta}$ is the yaw moment achieved from the lateral forces from the steered axle.

$$M_z = M_{zf} + M_{zr} + M_{z\delta} \tag{4.29a}$$

$$M_{zr} = \frac{T_r}{2R}(-T_{b,3} + T_{b,4} - G_{str}T_{EM,3} + G_{str}T_{EM,4}) = \frac{T_r}{2R}\Delta T_{ra} \tag{4.29b}$$

$$M_{zf} = \frac{T_f}{2R}(-T_{b,1} + T_{b,2} - G_{crs}T_{EM,1} + G_{crs}T_{EM,2}) = \frac{T_f}{2R}\Delta T_{fa} \tag{4.29c}$$

$$M_{z\delta} = 2C_{\alpha,f}L_f\delta_f \tag{4.29d}$$

The moment around the front axle, M_{steer}, is described by the differential force on the front wheels according to equation (4.30).

$$M_{steer} = r_s\Delta F_{xf} = r_s\frac{\Delta T_{fa}}{R} \tag{4.30}$$

The direct yaw moment (DYM) achieved by the differential torques can hence be written as equation (4.31).

$$M_{zf} = \frac{T_f}{2r_s}M_{Steer} \tag{4.31}$$

4.4.2.1 Motion Control - Steering Angle Based

A first approach to achieve steer by propulsion is to mainly control the longitudinal motion and steering angle. This system works for both a manual driver (using steer-by-wire or similar) and an AD system since it aims at tracking both the speed request and the input steering angle from the driver or AD system. The longitudinal control is chosen to be the same as for the previous method in equation (4.24). To provide a reference for the added global force M_{steer}, a PI controller was implemented in this case. A Volvo Transport Model (VTM) subsystem was used to generate a reference path to track, by simulating a driver model. To generate the required sum of moments about the front axle, the reference steering angle from the driver model is compared to the current estimated steering angle. The estimation is done by calculating the mean steering angle of the front left wheel and the front right wheel. This control scheme can be expressed as in equation (4.32d).

The yaw moment motion request is a combination of the yaw moment achieved by the current steer angle δ_{cf} and the requested change in steer angle. Hence, the yaw moment request is a combination of two parts, feedforward from the current steer angle and feedback from the steer angle controller that generates M_{steer} according to equation (4.32c) where $K_z = \frac{T_f}{2r_s}$. All the virtual forces for SBP are hence generated according to equation (4.32).

$$F_x[k] = K_{p,F_x}\Delta v_x[k] + K_{i,F_x}T_s\sum_{i=0}^{k}\Delta v_x[i] \tag{4.32a}$$

$$F_y[k] = 2C_{\alpha,f}\delta_{cf}[k] \tag{4.32b}$$

$$M_z[k] = 2C_{\alpha,f}L_f\delta_{cf}[k] + K_zM_{steer}[k] \tag{4.32c}$$

$$M_{steer}[k] = K_{p,s}\Delta\delta_f[k] + K_{i,s}T_s\sum_{i=0}^{k}\Delta\delta_f[i] \tag{4.32d}$$

The yaw moment could be further changed by adding feedforward of desired steer angle δ_f. The added yaw moment will be distributed differently depending on the weighting in the formulation of the control allocation. If the weighting is done such that the rear motors achieves the added yaw moment on their own, rapid yaw acceleration can be achieved due to the fast response of the electric motors.

4.4.2.2 Motion Control - Yaw Rate Based

A second approach is to achieve steer by propulsion based on a yaw rate controller. This method exploits the connection between the direct yaw moment and steering moment explained previously. However, it is designed for AD systems since the input steering angle is converted to a yaw rate reference based on a regular steered vehicle. The amplitude of the steering angle will be reduced as the differential torque will contribute with additional yaw moment. A steer-by-wire system can also handle a reduction in the requested steering angle. With a mechanical link, this is not possible since the steering output is physically linked to the steering wheel. Thus, a reduction in the steering angle would counteract the input from the driver. This would likely result in an undesirable driving experience. A steer-by-wire system simply handles this electronically. The yaw rate reference is generated according to equation (4.23) and a PI controller is used to generate DYM according to equation (4.33).

$$M_{DYM}[k] = K_{p,DYM}\Delta\omega_z[k] + K_{i,DYM}T_s\sum_{i=0}^{k}\Delta\omega_z[i] \tag{4.33}$$

The total yaw moment request is a combination of DYM and yaw moment from the current steering angle. Motion request for the longitudinal and lateral forces remains the same as for the steering angle-based approach. The yaw moment and steering moment are generated according to equation (4.34a) and equation (4.34b).

$$M_z[k] = 2C_{\alpha,f}L_f\delta_{cf}[k] + M_{DYM}[k] \tag{4.34a}$$

$$M_{steer}[k] = \frac{2r_s}{T_f}M_{DYM}[k] \tag{4.34b}$$

In this approach, a major difference is that the DYM is not limited to the front motors, but can be allocated onto all four motors. Limitations on the steering moment are described in the following subsection. These will provide limits on the DYM that is converted to steering moment. If the DYM is larger than what is physically possible from the front electric machines, the control allocation scheme will allocate the remaining moment to the motors on the rear axle.

4.4.2.3 Motion Control - LQR Yaw Rate Based

Finally, a third approach is to achieve steer by propulsion by using LQR. As in the previous approach, the control is based on the yaw rate and therefore mainly targeted for AD system functionality. The objective of an LQR is to minimize a cost function J with regards to weighting matrices for the states and inputs. This concept is described below in equation (4.35).

$$J = \sum_{k=0}^{\infty} x[k]^T Q_x x[k] + 2x[k]^T Q_{xu} u[k] + u[k]^T Q_u u[k] \tag{4.35}$$

The states are assumed to evolve according to the discrete state space model in equation (4.36).

$$x[k+1] = A_d x[k] + B_d u[k] \tag{4.36}$$

Design of the LQR therefore requires a state space model of the system that is intended to be controlled. In chapter 2, the single track model was introduced. The model will be extended with the model of the steering system in equation (2.28) that is repeated here for simplicity.

$$I_s\ddot{\delta}_f + b_s\dot{\delta}_f = M_{steer} - M_y - M_{resistive} \tag{4.37}$$

Modeling $\ddot{\delta}_f$ and $M_{resistive}$ as disturbances will reduce equation (4.37) to a first order differential equation. This simplification was also used in [21], which investigated a similar approach. An expression for M_y can be derived using the single track model approach and the definition of M_y in equation (2.27). Here, the sum of the mechanical trail and pneumatic trail are lumped into t_y.

$$M_y = t_y C_{\alpha,f}(-\delta_f + \beta + \frac{L_f\omega_z}{v_x}) \tag{4.38}$$

The equation of the steering system can now be written according to equation (4.39).

$$b_s\dot{\delta}_f = M_{steer} - t_y C_{\alpha,f}(-\delta_f + \beta + \frac{L_f\omega_z}{v_x}) \tag{4.39}$$

The single track model can be extended according to equation (4.40) where δ_f is instead a state and M_{steer} is the input.

$$\begin{bmatrix} \dot{\beta} \\ \dot{\omega}_z \\ \dot{\delta}_f \end{bmatrix} = \begin{bmatrix} \frac{-C_{\alpha,f}-C_{\alpha,r}}{mv_x} & \frac{-L_f C_{\alpha,f}+L_r C_{\alpha,r}}{mv_x^2} - 1 & \frac{C_{\alpha,f}}{mv_x} \\ \frac{-L_f C_{\alpha,f}+L_r C_{\alpha,r}}{I_{zz}} & \frac{-L_f^2 C_{\alpha,f}-L_r^2 C_{\alpha,r}}{I_{zz} v_x} & \frac{L_f C_{\alpha,f}}{I_{zz}} \\ \frac{t_y C_{\alpha,f}}{b_s} & \frac{t_y C_{\alpha,f} L_f}{b_s v_x} & -\frac{t_y C_{\alpha,f}}{b_s} \end{bmatrix} \begin{bmatrix} \beta \\ \omega_z \\ \delta_f \end{bmatrix} + \begin{bmatrix} 0 \\ \frac{T_f}{2 r_s I_{zz}} \\ \frac{1}{b_s} \end{bmatrix} M_{steer} \tag{4.40}$$

The state space model in equation (4.40) can be discretized and written on the form in equation (4.36). The yaw rate is chosen as the control variable and it can be expressed according to equation (4.41).

$$z[k] = \underbrace{\begin{bmatrix} 0 & 1 & 0 \end{bmatrix}}_{M} x[k] \tag{4.41}$$

Reference tracking with LQR control can be achieved in two different ways. The first solution is to use a reference gain and the second solution is to use integral action. The control law with reference gain can be defined according to equation (4.42).

$$u[k] = -Kx[k] + K_r r[k] \tag{4.42}$$

The reference gain is calculated for steady-state such that the steady-state error should be zero. The expression can be seen in equation (4.43).

$$\lim_{z \to 1} \frac{Z(z)}{R(z)} = I \tag{4.43}$$

The reference gain can finally be expressed as in equation (4.44).

$$K_r = (M(I - A_d + B_d K)^{-1} B_d)^{\dagger} \tag{4.44}$$

The other solution to achieve reference tracking is to add an integral state to the state space equation, shown in equation (4.45).

$$x_I[k+1] = x_I[k] + r[k] - z[k] \tag{4.45}$$

The state space model is thus augmented as seen in equation (4.46).

$$A_e = \begin{bmatrix} A_d & \mathbf{0} \\ -M & I \end{bmatrix} \tag{4.46a}$$

$$B_e = \begin{bmatrix} B_d \\ 0 \end{bmatrix} \tag{4.46b}$$

The control law in this case can then be expressed as in equation (4.47).

$$u[k] = \begin{bmatrix} K_x & \mathbf{0} \\ 0 & K_I \end{bmatrix} x[k] \tag{4.47}$$

Finally, the weighting matrices Q_x, Q_{xu} and Q_u are used to tune the control laws. It should be noted that the state space model is dependent on the linear velocity of the vehicle. In [20] an LQR controller for DYM was developed and it was concluded that for common operating velocities, $v_x > 5$ m/s, the difference in gains was negligible. A gain scheduled approach will therefore not be investigated in this thesis.

4.4.2.4 Steering Moment Limits

The moment about the steering axle that can be achieved from steer by propulsion is limited by the longitudinal tire forces as well as the scrub radius. In most driving conditions on high-μ surfaces, the motors will set the limits on M_{steer}. However, when driving on ice for instance, the limits will be set by the tire forces. This is since the maximum longitudinal force is determined by the normal force and the coefficient of friction, as shown in equation (4.11). The steering moment therefore needs to be dynamically limited by the motor and tire capabilities. To define the limits of SBP, the actuator dynamics constraints and tire force constraints that were described in section 4.3.3 and 4.3.4 will be used. The largest positive torque that can be applied to each of the front wheels are described according to equation (4.48).

$$T_{w,1}^{max} = T_{B,1}^{upper} + G_{crs} T_{EM,1}^{upper} \tag{4.48a}$$

$$T_{w,2}^{max} = T_{B,2}^{upper} + G_{crs} T_{EM,2}^{upper} \tag{4.48b}$$

The largest negative torque that can be applied can similarly be defined according to equation (4.49).

$$T_{w,1}^{min} = T_{B,1}^{lower} + G_{crs} T_{EM,1}^{lower} \tag{4.49a}$$

$$T_{w,2}^{min} = T_{B,2}^{lower} + G_{crs} T_{EM,2}^{lower} \tag{4.49b}$$

The upper and lower limits of M_{Steer} are expressed according to equation (4.50).

$$M_{steer}^{max} = \frac{r_s}{R}(T_{w,2}^{max} - T_{w,1}^{min}) \tag{4.50a}$$

$$M_{steer}^{min} = \frac{r_s}{R}(T_{w,2}^{min} - T_{w,1}^{max}) \tag{4.50b}$$

4.4.2.5 Control Allocation Formulation

To achieve the desired vehicle behavior of controlling the steering angle δ_f solely by using the front electric machines, one important limitation needs to be defined. Using this mode means that the power steering system is turned off, and thus, the steering angle is limited to the current steering angle when performing the CA optimization. In this way, only the front electric machines have the possibility to achieve the desired steering angle. This is described in equation (4.51).

$$\delta_{current} \leq \delta_f \leq \delta_{current} \tag{4.51}$$

Locking the steering angle request results in F_y becoming redundant to include in the optimization, since only the steering angle can affect F_y. Thus, the weight of F_y can be set to zero to practically omit the virtual force in the CA optimization. Also, only the differential torque and its contribution to the moment around the kingpin axles will be considered. This is due to the fact that δ_f would become a control input and state in the formulation. The interpretation of M_{steer} might become a bit peculiar but it is considered as a virtual force that makes it possible to steer the front axle and it creates a direct yaw moment. The uncertainties of the steering system is handled by the closed loop control. The complete set of virtual forces that will be used in the SBP formulation are shown in equation (4.52).

$$\mathbf{v} = \begin{bmatrix} \mathbf{F}_x \\ \mathbf{F}_y \\ \mathbf{M}_z \\ \mathbf{M}_{steer} \end{bmatrix} \tag{4.52}$$

The control effectiveness matrix is defined according to equation (4.53).

$$B = \begin{bmatrix} \frac{1}{R} & \frac{1}{R} & \frac{1}{R} & \frac{1}{R} & \frac{G_{crs}}{R} & \frac{G_{crs}}{R} & \frac{G_{str}}{R} & \frac{G_{str}}{R} & 0 \\ 0 & 0 & 0 & 0 & 0 & 0 & 0 & 0 & 2C_{\alpha,f} \\ \frac{-T}{2R} & \frac{T}{2R} & \frac{-T}{2R} & \frac{T}{2R} & \frac{-TG_{crs}}{2R} & \frac{TG_{crs}}{2R} & \frac{-TG_{str}}{2R} & \frac{TG_{str}}{2R} & 2L_f C_{\alpha,f} \\ \frac{-r_s}{R} & \frac{r_s}{R} & 0 & 0 & \frac{-G_{crs}r_s}{R} & \frac{G_{crs}r_s}{R} & 0 & 0 & 0 \end{bmatrix} \tag{4.53}$$

4.4.2.6 Steering Angle Modification

Steer by propulsion can change the steering characteristics of the vehicle as mentioned earlier. The differential torque will add yaw moment for the same steering angle compared to regular steering. One steer angle based approach and two yaw rate based approaches were proposed for motion control. To achieve similar behavior between the three methods, a proposed method is to change the steering angle reference to achieve similar yaw rate as when using regular steering. In chapter 2 the single track model was introduced, this model can be extended to include direct yaw moment added from differential torques on the wheels according to equation (4.54).

$$\begin{bmatrix} \dot{\beta} \\ \dot{\omega}_z \end{bmatrix} = \begin{bmatrix} \frac{-C_{\alpha,f}-C_{\alpha,r}}{mv_x} & \frac{-L_f C_{\alpha,f}+L_r C_{\alpha,r}}{mv_x^2} - 1 \\ \frac{-L_f C_{\alpha,f}+L_r C_{\alpha,r}}{I_{zz}v_x} & \frac{-L_f^2 C_{\alpha,f}-L_r^2 C_{\alpha,r}}{I_{zz}v_x} \end{bmatrix} \begin{bmatrix} \beta \\ \omega_z \end{bmatrix} + \begin{bmatrix} \frac{C_{\alpha,f}}{mv_x} & 0 \\ \frac{L_f C_{\alpha,f}}{I_{zz}} & \frac{1}{I_{zz}} \end{bmatrix} \begin{bmatrix} \delta_f \\ M_{DYM} \end{bmatrix} \tag{4.54}$$

If the direct yaw moment, M_{DYM}, is applied on the front wheels, it will also affect the steering angle δ_f. In the design of steer by braking [13], an approach using the rigid body dynamics and steering system equation at steady state was used to modify the yaw rate and steering angle. The approach in equation (4.54) will therefore also be to solve the equations for steady state and hence neglect the relation between M_{DYM} and δ_f. Equation (2.15) and (4.54) can be solved for ω_z at steady state ($\dot{v}_y = 0$ and $\dot{\omega}_z = 0$). To achieve the same yaw rate, the equations can be set equal and the steering angle from equation (4.54) can be expressed according to equation (4.55).

$$\delta_f^{M_{DYM}} = \delta_f - \frac{C_{\alpha,r} + C_{\alpha,f}}{C_{\alpha,f} C_{\alpha,r} L} M_{DYM} \tag{4.55}$$

The steering angle request, $\delta_f^{M_{DYM}}$, will therefore be calculated from the driver input, δ_f, and the current direct yaw moment, M_{DYM}.

4.4.3 Modeling Of Energy Consumption

In order to compare the energy consumption of using SBP, with using only power steering, a simplified model is used. This allows for utilizing data from the VTM model used in simulations. In a rotational sense, power can be defined as in equation (4.56). Thus, a simple estimation is to calculate the power consumption of each wheel during a simulation. This can be applied when using SBP.

$$P_{wheels} = T\omega \tag{4.56}$$

In the case of using only power steering, the power consumption of the steering system also has to be taken into account. Thus, the total power consumption in this case is the sum of the wheel consumption as well as the consumption of the steering system according to equation (4.57).

$$P_{tot} = P_{wheels} + P_{steer} \tag{4.57}$$

Due to the limitations of the VTM model, the torques from the power steering was modeled as seen in equation (4.58).

$$T = M_{wz} + t_m F_{wy} \tag{4.58}$$

Here, the torque consists of the moment about the z-axis of each front tire, as well as the the torque needed due to the caster offset. To obtain the power consumed by the power steering, this total torque can then be multiplied with the rate of change of the front axle steering angle. The final expression can be seen in equation (4.59), where η_{ss} is the efficiency of the steering system.

$$P_{steer} = \frac{2|(M_{wz} + t_m F_{wy})\dot{\delta}_f|}{\eta_{ss}} \tag{4.59}$$

4.5 Wheel Controllers

Each motor is controlled individually and this section provides insight how this is done. The wheels are also controlled with service brakes that have slower dynamics than the motors. The electric motors are intended to be controlled using an interface by Volvo which is named individual Xternal Propulsion Request (iXPR) and accepts two different requests. Wheel speed can be requested with torque limits, and torque can be requested with wheel speed limits. To be able to simulate the system, a similar interface was developed in the simulation environment for the simplified actuator models.

4.5.1 Wheel Speed Control

Each wheel unit is provided with a PI controller to regulate the speed based on a reference provided by the CA. The torque request from the CA can be converted to wheel speed using various methods. The PI controller acts on the error calculated by measuring the wheel speed and subtracting it from the reference speed. A desired behavior can be achieved by tuning the controller using step responses. The output from the controller is a torque input to the motor model. Due to physical limitations, a limit in the controller needs to be included. Hard limits are provided by the motor maps as it defines the operating range. A lookup table for the current wheel speed can be used to limit the output. Desired limits requested by the CA for e.g reducing slip can be provided and needs to fall within the hard limits. The implementation of the speed controller is done according to equation (4.60) where the limits are provided as described.

$$T^{req}[k] = K_{p,\omega}(\omega^{ref}[k] - \omega[k]) + K_{i,\omega} T_s \sum_{i=0}^{k} (\omega^{ref}[i] - \omega[i]) \tag{4.60a}$$

$$T[k] = \begin{cases} T^{max}, & T^{req}[k] \geq T^{max} \\ T^{req}[k], & T^{min} \leq T^{req}[k] \leq T^{max} \\ T^{min}, & T^{req}[k] \leq T^{min} \end{cases} \tag{4.60b}$$

4.5.2 Wheel Torque Control

The torque control of the motors is provided with a slip limiter function to provide an extra layer of safety and stability control of the vehicle. The purpose of the slip controller is to reduce the wheel slippage in case the control allocator is requesting more wheel force that the tire can handle. This could occur if there are estimation errors from the motion estimation layer which provides the control allocator with too large limits. This is an indirect form of torque control with speed limits, since the slip can be related to wheel speed. The implementation is done according to equation (4.61).

$$T^{upper}[k] = K_{p,T}(s_x^{upper}[k] - s_x[k]) + K_{i,T}T_s \sum_{i=0}^{k}(s_x^{upper}[i] - s_x[i]) \tag{4.61a}$$

$$T^{lower}[k] = K_{p,T}(s_x^{lower}[k] - s_x[k]) + K_{i,T}T_s \sum_{i=0}^{k}(s_x^{lower}[i] - s_x[i]) \tag{4.61b}$$

$$T[k] = \begin{cases} T^{upper}, & T^{CA}[k] \geq T^{upper} \\ T^{CA}[k], & T^{lower} \leq T^{CA}[k] \leq T^{upper} \\ T^{lower}, & T^{CA}[k] \leq T^{lower} \end{cases} \tag{4.61c}$$

5
Simulations

In this chapter, simulations with the control designs presented in chapter 4 are evaluated. These simulations are performed on a VTM model, where the dynamics of the plant model are provided by Volvo. First, a test case on ice is simulated to test the slip performance of the wheel controller. Thereafter, the implementation of steer by propulsion is tested and evaluated. The different approaches presented in section 4.4.2 are compared in a maneuverability test using the Stanley controller. The rest of the test cases are for the steering angle-based approach since it is the most general method. These test cases are evaluated using the VTM driver model to further illustrate that the control methods are valid for different input sources. It should be noted that torque distribution using control allocation is not simulated here, since the main purpose of this thesis is to investigate steer by propulsion. Finally, an energy consumption comparison is done between a vehicle model using steer by propulsion, and a vehicle using solely electric power steering.

5.1 Wheel Controller Slip Performance

The wheel controllers with slip limits are mainly to add an extra layer of safety and stability. Figure 5.1 shows how the wheel controllers limit the longitudinal slip on each wheel. Here, an acceleration of 1 m/s^2 is requested on an icy road. Furthermore, for illustrative purposes, the CA is provided with a coefficient of friction corresponding to dry asphalt. Therefore, the high level controllers will allocate higher torques than the wheels can handle on the icy surface. This test will illustrate how the low level controllers can intervene in such cases, and limit the torque according to a given slip limit. In this case, only the tractor is considered. It can therefore be observed that mainly the front motors are handling the propulsion request. When the longitudinal slip on the front tires reaches a level of 0.2, indicated by dashed lines in the figure, the wheel controllers are engaged to saturate the torque in order to keep the slip limited to its set maximum level. The corresponding torques can be seen in figure 5.2, where the request from the CA is reduced in the actual output torque in order to satisfy the slip limits. As can be seen in this figure, the requested torques on the front left wheel and the front right wheel are different. This is since the slip seems to cause a slight drift to the left, and since SBP is the method used here, it will try to compensate by achieving a slight turn to the right. Thus, it can also be noted the low level controllers cannot affect lateral forces directly.

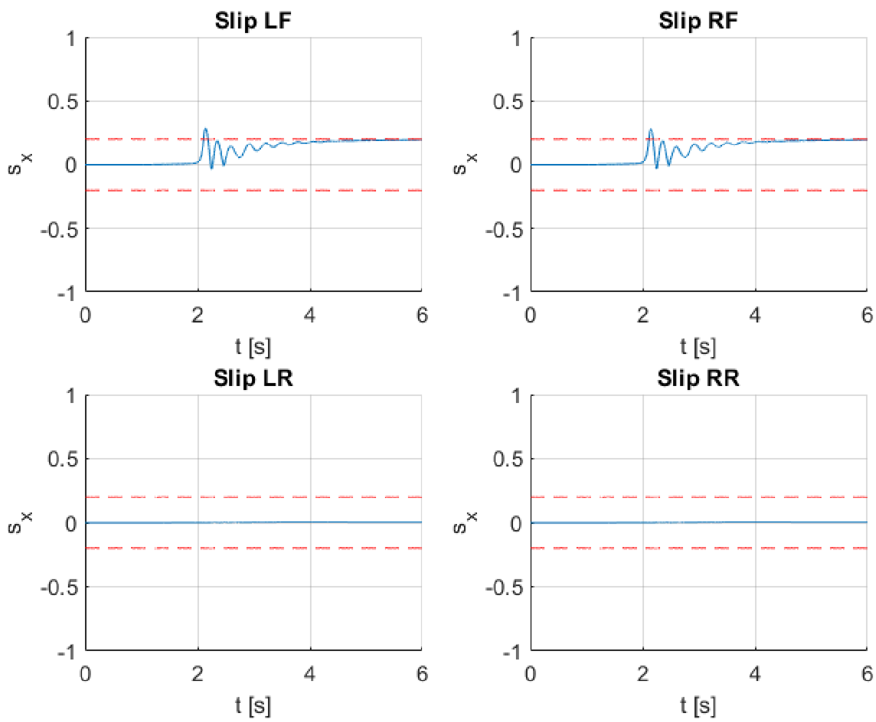

Figure 5.1: Longitudinal slip on each wheel. Dashed lines indicate the slip limit, which in this case is set to 0.2.

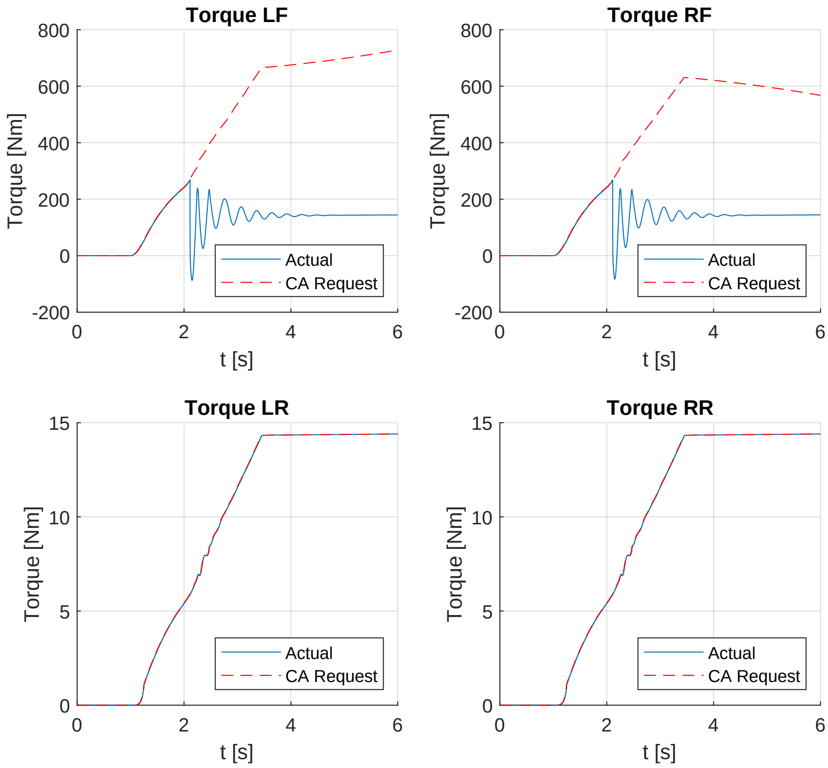

Figure 5.2: Corresponding torques on each wheel in the slip performance test. Blue indicates the actual output torque, while the dashed line indicates the request from the control allocator.

5.2 Steer By Propulsion Performance

Firstly, the performance and maneuverability of SBP is tested on a tractor by itself. Since the tractor is the controlled unit of the vehicle, it is appropriate to test the handling capabilities by itself. Thereafter, a number of common driving scenarios are tested with a semitrailer added for completeness.

5.2.1 Cornering Test Cases

The maneuverability of the tractor was tested in several different scenarios. The chosen example that is illustrated in this section highlights the differences in performance between the various control strategies. In the example, the Stanley controller is used to follow a given path with a 75 m radius while the vehicle should remain at a longitudinal speed of 40 km/h. The test curve can be observed in figure 5.3 and the vehicle reaches a lateral acceleration of 1-2 m/s^2. The critical parts of the cornering test are entering, staying in the curve and exiting the curve. It should also be noted that the test is performed on dry asphalt. Similar tests were made on roads with lower coefficient of friction, where the maximum lateral acceleration is lower due to the available friction forces. In those cases, the vehicle would need to slow down in order to perform the same maneuver.

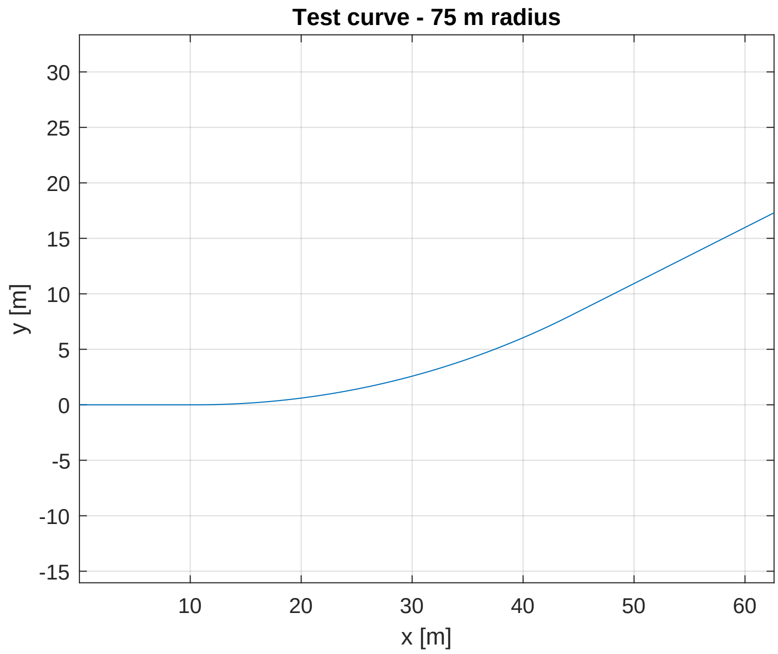

Figure 5.3: Test track for the cornering test.

In figure 5.4, the performance of the steering angle-based approach can be observed. From the plots of the steering angle it can be observed that the reference is tracked with relatively high accuracy. However, to follow the constant radius, an oscillatory behavior on the steering command occurs. Previously it was discussed that SBP can change the driving characteristics which probably causes the slight oscillatory behavior in this case. It can also be seen how the yaw rate lags behind the reference provided by the the reference model.

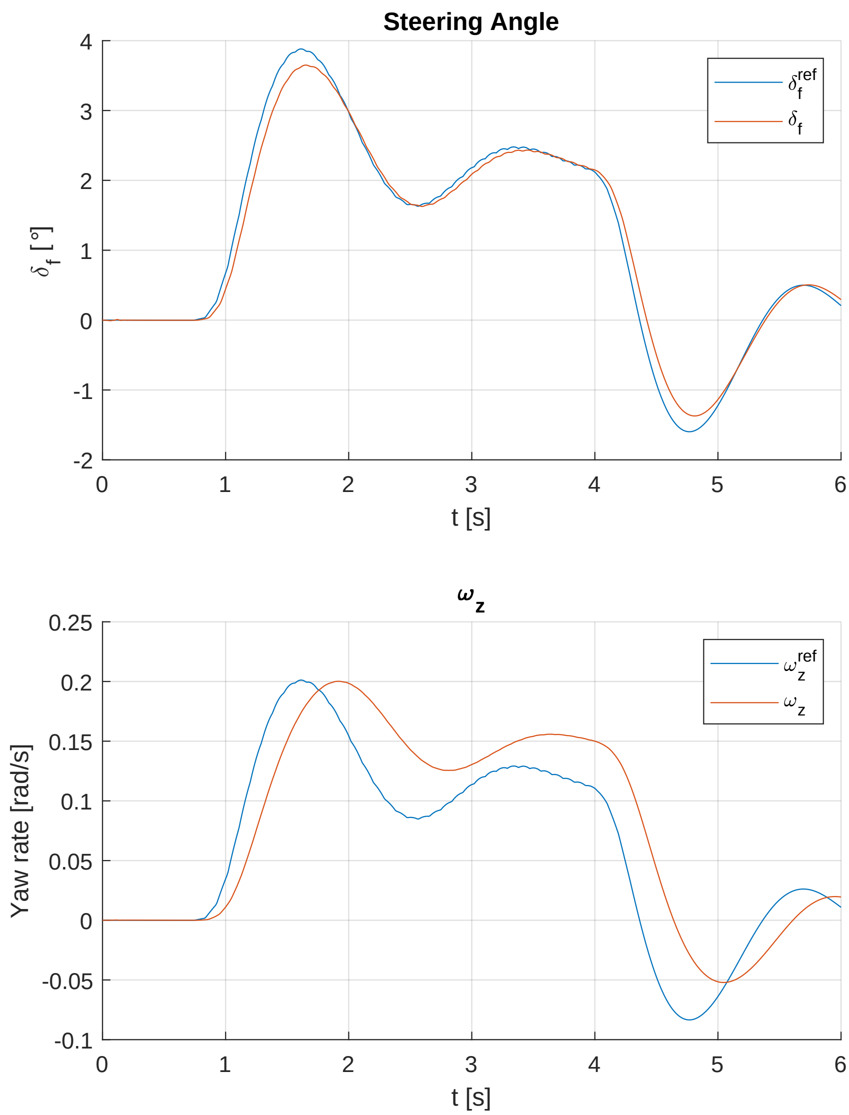

Figure 5.4: Actual steering angle and yaw rate compared to references in the case of using steering angle-based control.

In figure 5.5, a less oscillatory behavior in steering command is observed compared to the steering angle-based approach. Here, it can be seen that the steering angle request is reduced in order to track the yaw rate reference. Thus, this could provide a driver with a more expected vehicle behavior.

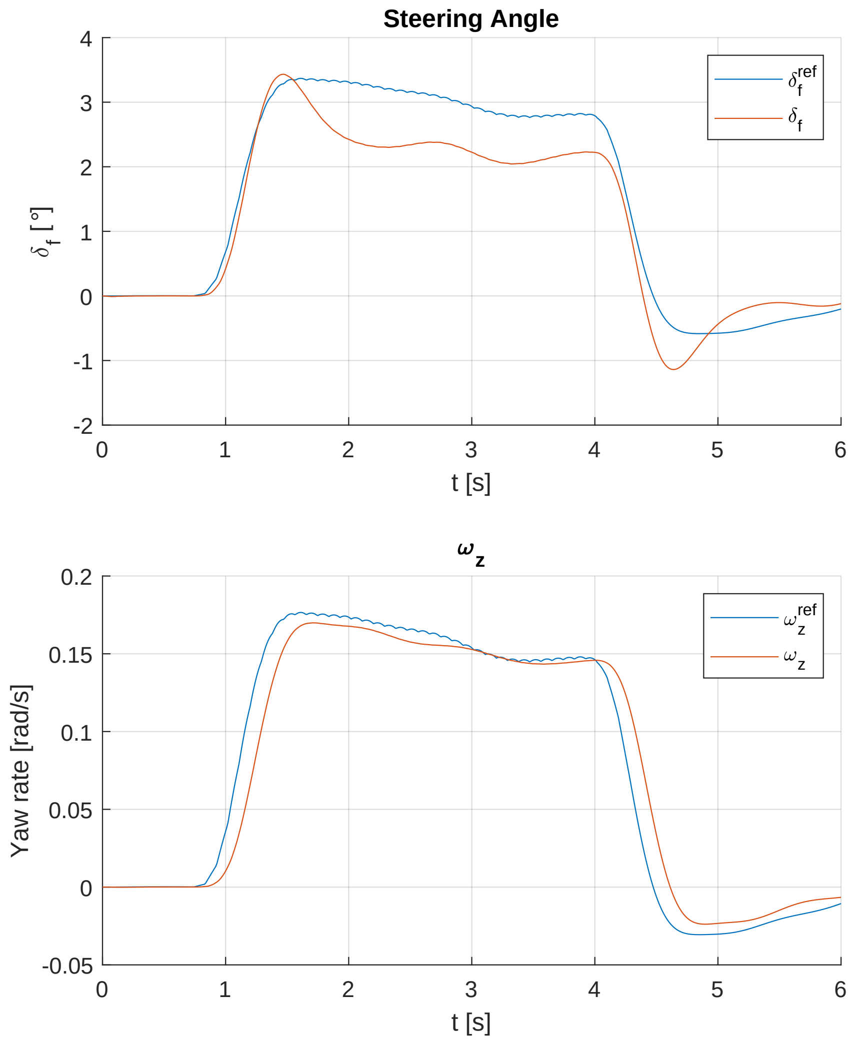

Figure 5.5: Actual steering angle and yaw rate compared to references in the case of using yaw rate-based control with PI.

In figure 5.6, the approach using LQR with reference gain can be observed. It can be noted that the steering command is slightly more oscillating compared to the yaw rate-based PI approach. However, the steering angle is still reduced in this case as well in order to track the yaw rate. Furthermore, a slight delay is also observed in the yaw rate tracking. In this case, the reference gain is more directly coupled to the steering command. This method essentially only uses a proportional gain, in contrast to the PI, which has an integral part as well.

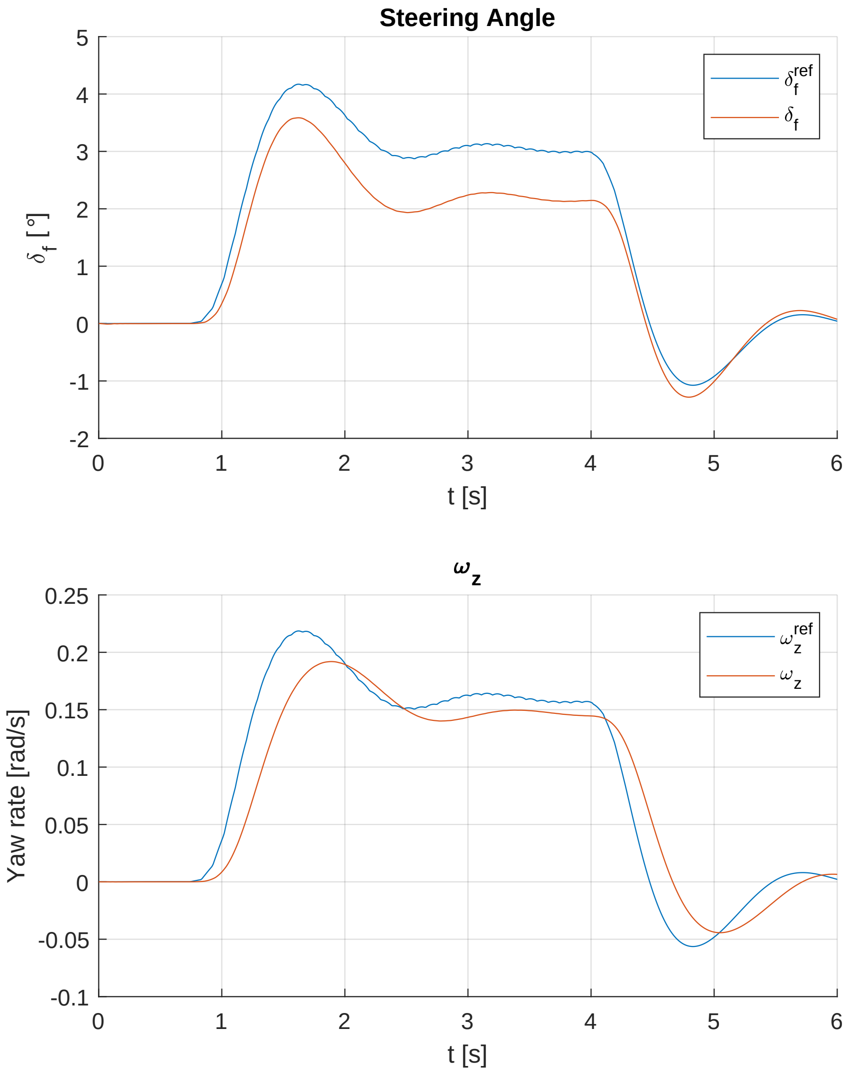

Figure 5.6: Actual steering angle and yaw rate compared to references in the case of using yaw rate-based control with LQR using reference gain.

In figure 5.7, the approach using LQR with integral action can be observed. Compared to the previous approach with reference gain, it can be seen that the yaw rate is tracked with improved accuracy. Furthermore, the steering command is smooth as expected for a constant turn, in comparison to the previous approaches, where a slight oscillatory behavior is present.

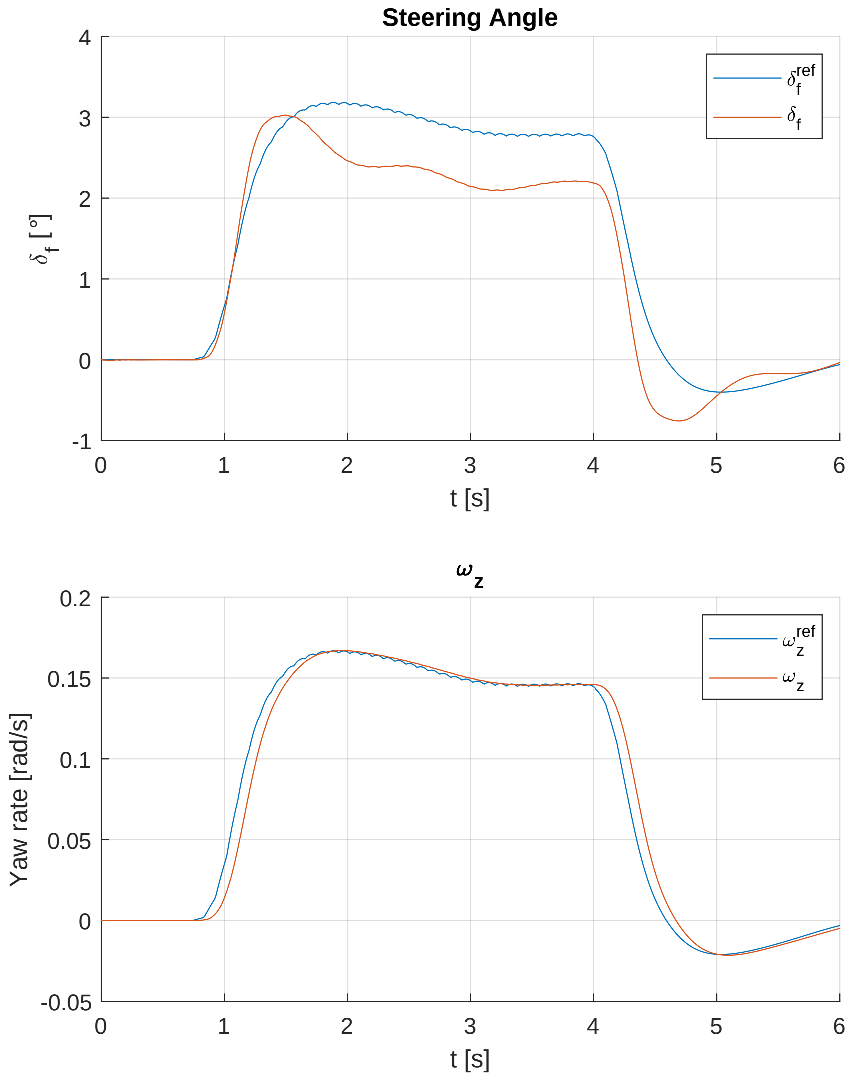

Figure 5.7: Actual steering angle and yaw rate compared to references in the case of using yaw rate-based control with LQR using integral action.

Finally, in figure 5.8 the steering angle-based method with reduced reference is shown. The steering command is in this case shown in green while the reduced reference is illustrated in blue. It is clear that the oscillatory behavior is large in this case. The tracking of the yaw rate is also poor.

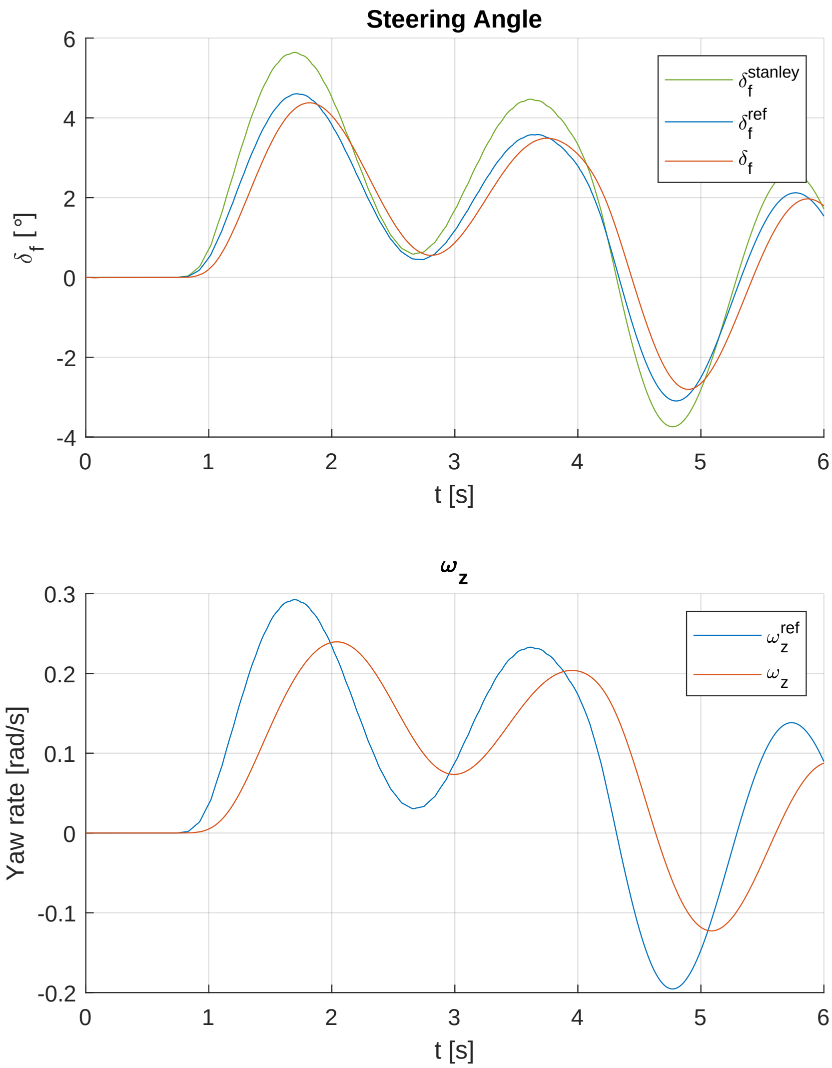

Figure 5.8: Actual steering angle and yaw rate compared to references in the case of using steering angle-based control with a modified steering angle.

The steering command and yaw rate illustrates the differences in vehicle behavior. It is also relevant to observe how well the vehicle tracks a given path using the different control strategies. Lateral offset is used to measure the performance. In figure 5.9, the lateral offset can be seen for each respective control approach in the given test case. Note that the Stanley controller is fairly simple and that part of the tracking error could be due to the performance of the path follower. Since all SBP control strategies were evaluated using the same controller, this potential error would be inherent for all. The comparison is therefore deemed to be fair. In the figure, it can be seen that all methods except the last are performing on a similar level, in regards to lateral offset.

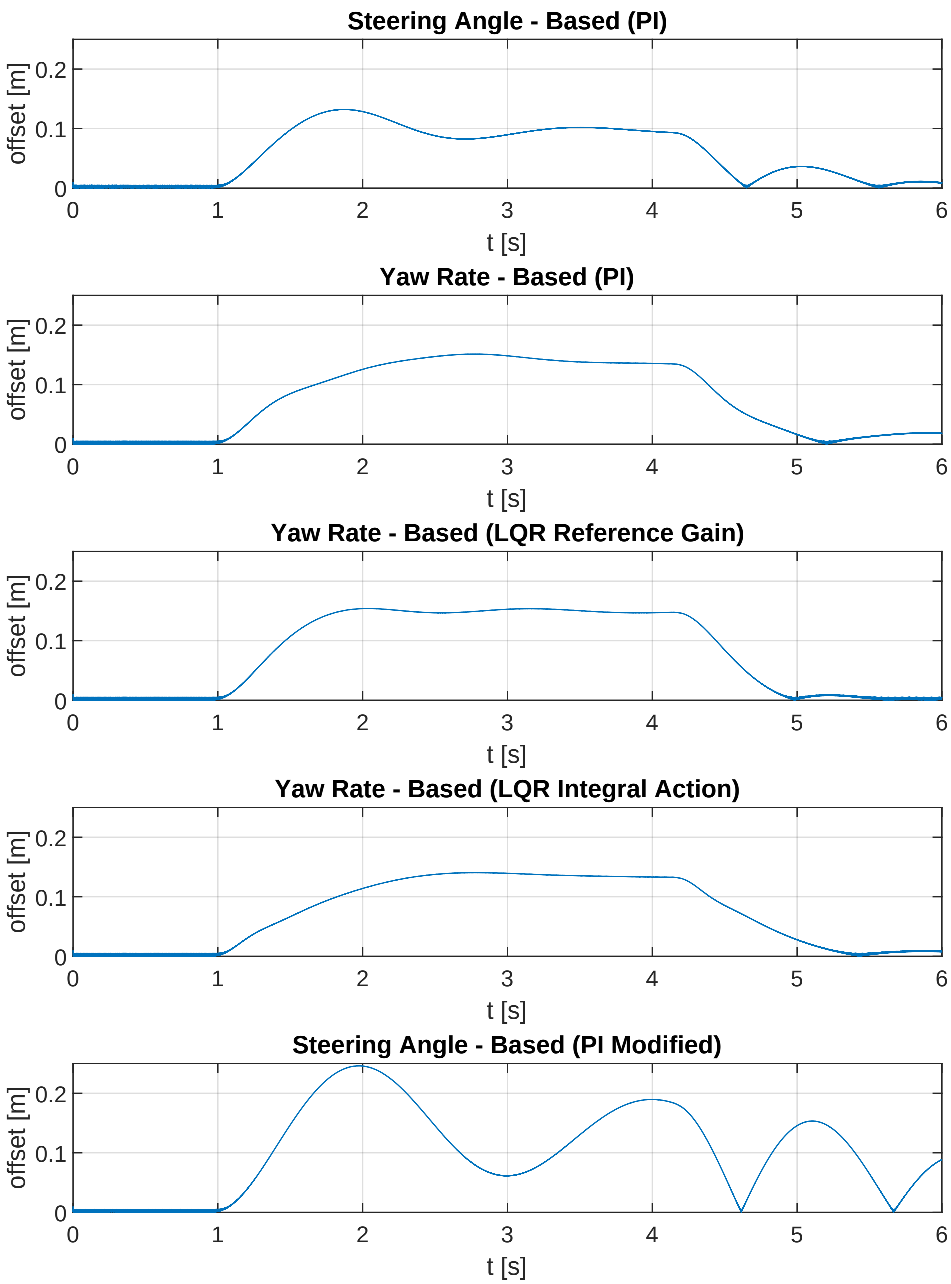

Figure 5.9: Lateral offset for each respective control approach in the given test case.

The two steering angle-based approaches can be seen to have a more prominent oscillatory behavior, compared to the yaw rate-based methods. It should also be noted that the LQR with reference gain displayed a slight oscillatory behavior. As mentioned earlier, this is likely due to the lack of any integral action. Furthermore, it can be seen that the achieved yaw rate of the steering angle-based methods lag behind the reference model. This is probably due to the mechanical inertia of the steering system. An applied differential torque on the front axle will give a direct yaw moment within a number of milliseconds due to the dynamics of the motors, which will result in a yaw moment. Simultaneously, this will cause the steering system to turn, adding further yaw moment to the vehicle. However, the time delay of the steering system is significantly larger. Thus, the combined effect is not synchronized as the turning will be amplified when the wheels have started to turn. Therefore, the driver or path follower would likely experience more cornering than expected, implying a counteracting motion is needed. The nature of the two different time delays in the system can make this difficult to handle. This will result in an oscillatory behavior in regards to the tracking of the desired path. The modified steering angle approach did not work as intended when derived. This is likely due to the aforementioned time delays in the system making the dynamics rather complicated and not as simple as lowering the steering command to achieve a reference yaw rate.

The yaw rate methods using the integral action displayed smooth driving behavior in the sense of yaw rate tracking. Steering commands from the path follower is less oscillatory. In both cases with integral action it can be observed how the achieved steering angle rapidly peaks, to then slowly settle at a lower level. During this period the steering command from the path follower remains more or less the same. The controllers show how the different time delays are handled internally thanks to the models of the system as well as the integral action. The yaw rate considers the whole vehicle motion in contrast to the steering angle control, which only considers the yaw moment about the front axle. The fast response of the electric motors can therefore be used to handle high frequency changes, allowing for corrections much faster than a path follower or driver.

The steering angle-based approach is simpler in the sense that it does not require detailed information about the states of the vehicle. Yaw rate-based methods provide better driving behavior, but require more data on the vehicle states and are based on simplified models. Since the lateral offsets are on a similar magnitude with these approaches, the steering angle-based approach is recommended to use due to its simplicity and versatility.

5.2.2 Test Scenarios Using Steering Angle-Based Approach

A first test case with the semitrailer added is illustrated in figure 5.10, where a turn in constant radius is performed at 30 km/h. It can be observed that the desired path is achieved with a lateral offset on a magnitude of centimeters. Here, the position of front axle is compared to the desired path to obtain the lateral offset. The largest offset can mainly be seen when changes in the steering angle is requested. This is likely due to the small time delay when trying to achieve the corresponding moment about the front axle. At lower speeds, this issue is less noticeable though.

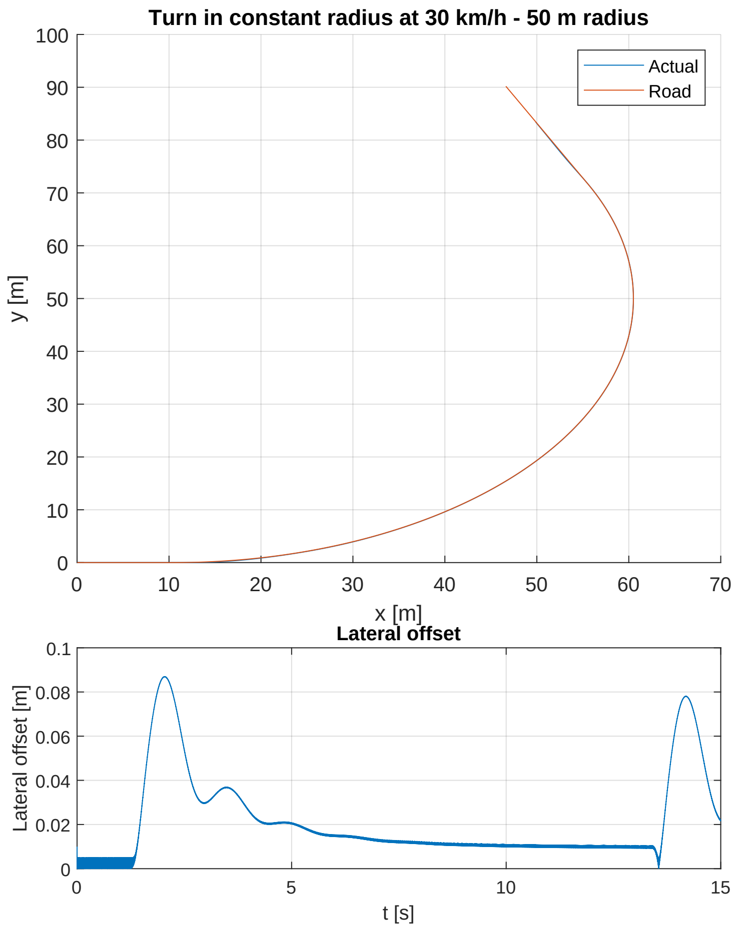

Figure 5.10: Simulation of turn in constant radius of 50 m at 30 km/h. Lateral offset between the desired and actual path is seen below.

In figure 5.11, the resulting motor torques can be seen for the test case above. It can be seen that the desired behavior is achieved, in the sense that the left motor on the front axle is regenerating energy when performing a left turn, while the right motor is providing extra torque to achieve the turn. The motors on the rear axle are providing small torques to assist in the longitudinal propulsion, and the weighting for these motors can be slightly reduced when performing cornering. This allows for the front motors to focus on achieving the desired moment about the front axle, rather than trying to achieve the desired longitudinal propulsion simultaneously.

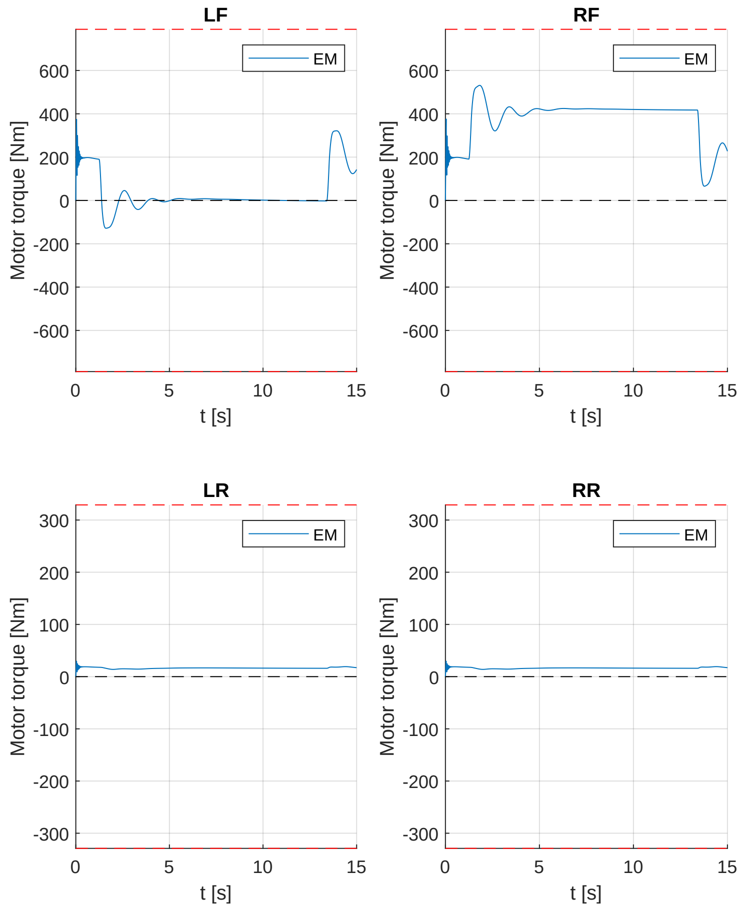

Figure 5.11: Motor torques in simulation of turn in constant radius of 50 m at 30 km/h. Dynamic limits are indicated by dashed lines.

The performance of SBP is reduced when increasing the vehicle speed. In this second simulation, figure 5.12 illustrates a turn in constant radius of 100 m at 50 km/h. A more oscillating behavior can be observed in the lateral offset when performing cornering. This is likely due to the aforementioned issue with time delay. Also, the front motors are trying to achieve the requested moment and the longitudinal propulsion at the same time.

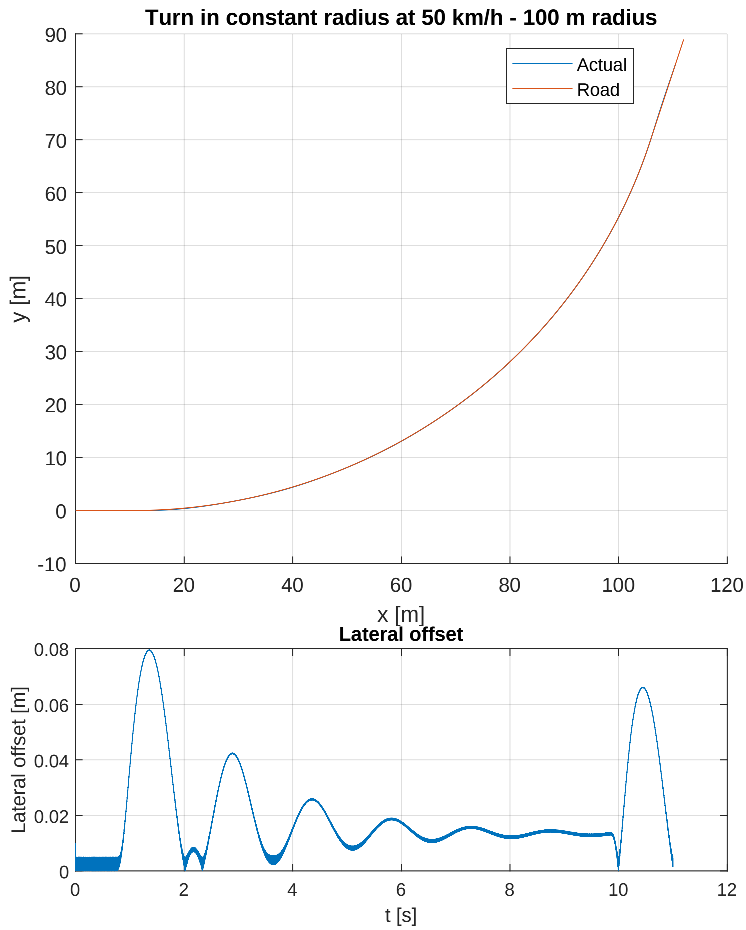

Figure 5.12: Simulation of turn in constant radius of 100 m at 50 km/h. Lateral offset between the desired and actual path is seen below.

The oscillating behavior is further observed in the corresponding motor torques in figure 5.13. However, the SBP scheme still manages to allocate torques in a similar manner to the previous test case.

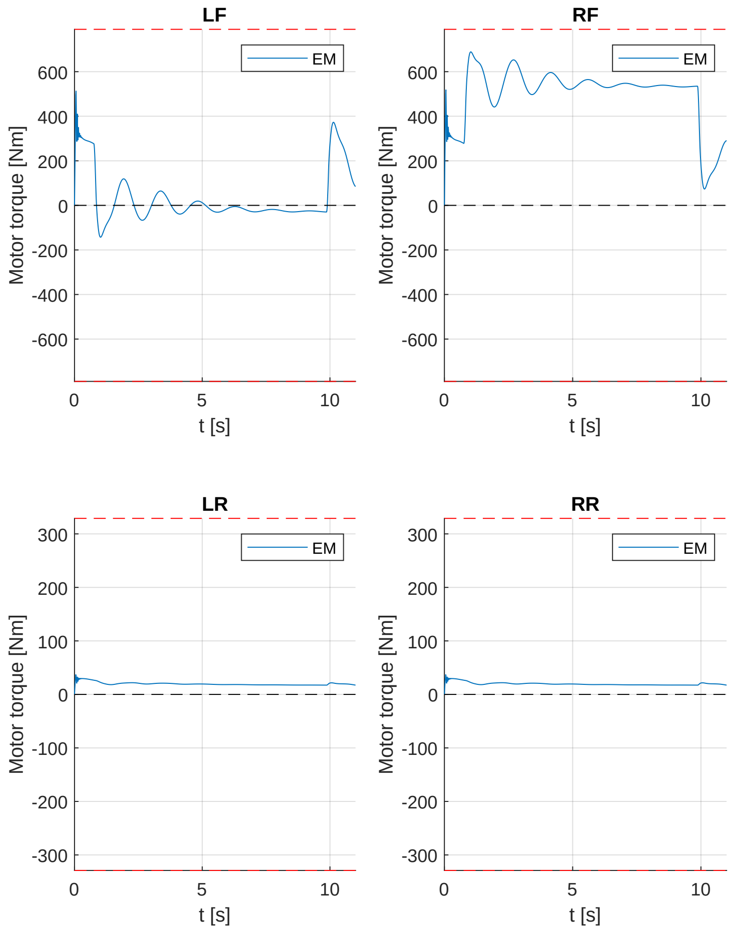

Figure 5.13: Motor torques in simulation of turn in constant radius of 100 m at 50 km/h. Dynamic limits are indicated by dashed lines.

The capabilities of SBP are not fully limited to lower speeds, however. In figure 5.14, a lane change at 85 km/h is illustrated. The desired path is followed relatively well, but as shown in figure 5.12, higher speeds create a more oscillating behavior in the lateral offset.

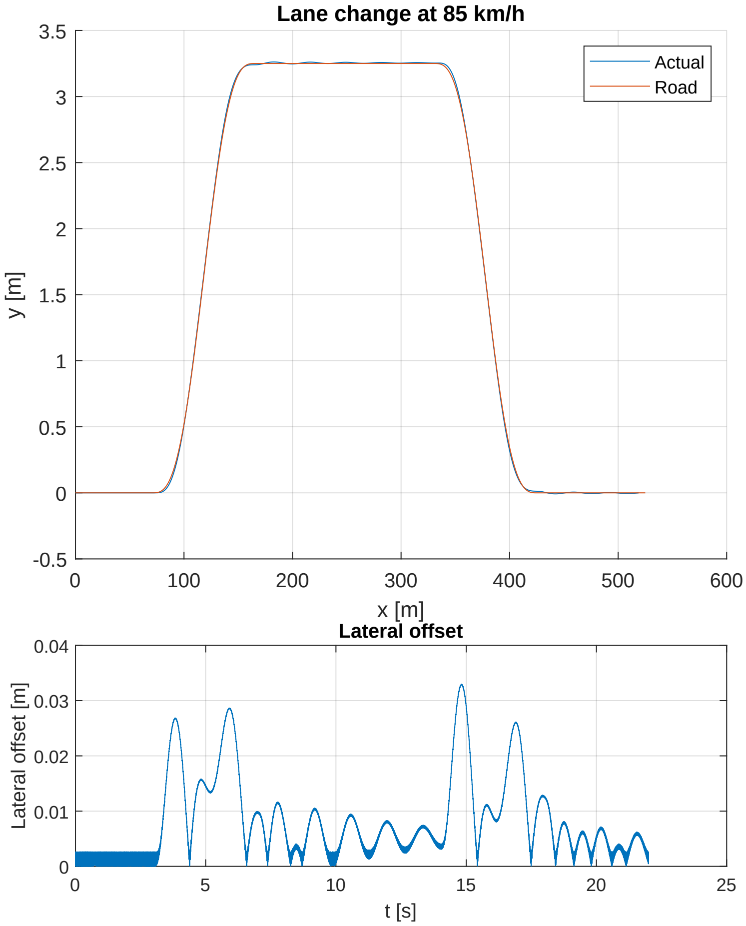

Figure 5.14: Simulation of lane change at 85 km/h.

In figure 5.15, the corresponding motor torques are displayed. As previously, the front motors first achieve a difference in torque to perform the lane change. Thereafter, the motors provide the same amount of torque to propel the vehicle straight forward. Finally, a difference in torque is achieved once again to move the vehicle back to the original lane. Meanwhile, the rear motors provide a small amount of torque to keep the longitudinal velocity at 85 km/h.

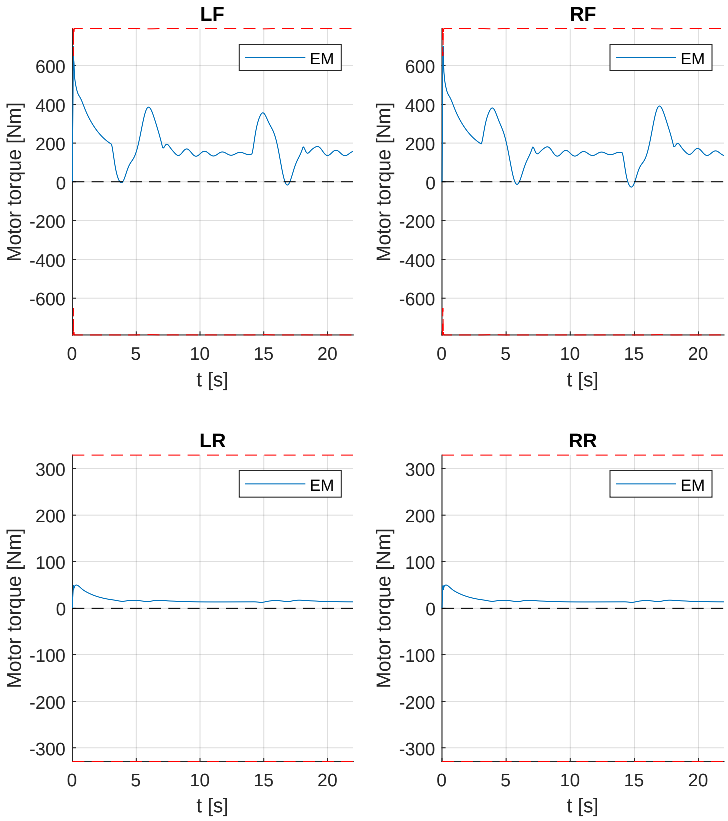

Figure 5.15: Motor torques of lane change at 85 km/h.

Overall, the performance of the vehicle is improved using SBP compared with using power steering, in the sense of lateral offset. With increased vehicle speed, a more oscillating behavior is observed. Thus, from a stability point of view, it is more appropriate to use SBP mainly at lower speed. If motion estimation and parameters are known, it is worthwhile to consider using the yaw rate-based methods. However, these methods will require a model for each vehicle combination, making the implementation more difficult.

5.3 Energy Consumption Comparison

Using the modeling of the energy consumption in 4.4.3, a number of test cases are chosen to compare SBP (steering angle-based) with using power steering only. This is done in order to compare with how a standard 4WD vehicle would allocate the torque. Here, the torque allocation for the power steering case is based on a simple approach where the requested longitudinal force F_x is split evenly between all wheels. Hence, there is no torque vectoring done in this case and the steering angle is controlled solely by the power steering unit. Here, the tests are performed for the tractor only, since this is the controlled unit. The situations where changes in energy consumption can be observed is mainly in short maneuvers over a few seconds where the vehicle is performing some type of cornering. Thus, the two first tests are simulated for 10 s, while the final lane change test is simulated for 22 s to also illustrate a longer maneuver.

In table 5.1, the energy consumption can be observed in the case of a turn in constant radius R = 50 m with an initial velocity of 50 km/h. This test is chosen to illustrate how a truck exits a highway while braking and turning in a curve. By using SBP it can be seen that the energy consumption is increased by 3.8 % in this driving scenario, as we regenerate less energy than using power steering. It can be seen in the SBP case that the difference in consumption of the two front motors is relatively large. This suggests that the needed moment to achieve the requested steering angle requires more power than using power steering in this case. Since the weighting of the motors in the SBP case is based on the concept that the front motors should be prioritized, this means that the rear motors cannot regenerate as much as in the power steering case.

Brake in turn with constant radius R = 50 m	SBP	Power steering
Left front wheel [kWh]	-0.072	-0.015
Right front wheel [kWh]	0.019	-0.016
Left rear wheel [kWh]	-0.003	-0.016
Right rear wheel [kWh]	-0.003	-0.016
Total consumption [kWh]	-0.0598	-0.0621
Ratio of consumption SBP/Power steering [%]	3.8	

Table 5.1: Energy consumption in the case of a braking in a turn in constant radius R = 50 m, with initial velocity of 50 km/h.

In table 5.2, the energy consumption can be observed in the case of a turn in constant radius R = 100 m at 50 km/h. This test is chosen to illustrate the differences in consumption when performing cornering at a constant speed. By using SBP in this case, the energy consumption is increased by 3.6 %. In this scenario, similar arguments can be made as in the previous case. Here, the rear motors in the SBP case are not allowed to be used as much as in the power steering case, due to the weighting. Thus, the front motors are trying to achieve the needed moment about the front axle, as well as handling the majority of the longitudinal propulsion.

Turn in constant radius R = 100 m at 50 km/h	SBP	Power steering
Left front wheel [kWh]	-0.036	0.017
Right front wheel [kWh]	0.101	0.017
Left rear wheel [kWh]	0.002	0.016
Right rear wheel [kWh]	0.002	0.016
Total consumption [kWh]	0.0686	0.0662
Ratio of consumption SBP/Power steering [%]	3.6	

Table 5.2: Energy consumption in the case of a turn in constant radius R = 100 m at 50 km/h.

Finally, a lane change at 85 km/h is simulated to show how the consumption differs at higher speeds with less cornering. Table 5.3 shows the energy consumption in this case. Here, it can be observed that SBP increases the consumption by 2.1 % compared to using power steering. Here, it can be noted that the difference in consumption is less than in the previous cases. This is likely because less cornering is performed, which can be seen in the consumption of the front motors in the SBP case. Hence, these simulations indicate that achieving the desired steering angle using SBP increases the energy consumption slightly.

Lane change at 85 km/h	SBP	Power steering
Left front wheel [kWh]	0.082	0.047
Right front wheel [kWh]	0.083	0.047
Left rear wheel [kWh]	0.008	0.042
Right rear wheel [kWh]	0.008	0.042
Total consumption [kWh]	0.1804	0.1766
Ratio of consumption SBP/Power steering [%]	2.1	

Table 5.3: Energy consumption in the case of a lane change at 85 km/h.

The comparison of the energy consumption therefore shows that SBP consumes a few percent of additional energy than using only power steering in all tested cases. One proposal is to change the weighting in the SBP case when performing cornering, in order to allow higher use of the rear motors in this case. This will, for instance, allow for higher total regeneration in the SBP case. However, it seems that most of the difference in consumption originates from the steering mechanics. This is difficult to improve with the control system or the actuators. Rather, this is a question of mechanical design of the truck, where an increased scrub radius could deliver a higher moment with the same difference in forces of the front wheels. However, there is also a trade-off in this case as the handling and driver comfort would be affected.

6
Conclusions

In this final chapter, the research questions presented in chapter 1 are reviewed and analyzed. Suggestions for future works are also provided.

To conduct the conclusion of the thesis, the research questions are recalled as follows:

- How can the optimal control scheme be formulated for the chosen powertrain configuration, application and electric machine interface?
- How can steer by propulsion influence vehicle performance and what are its limitations?
- Compared with using power steering, how is the energy consumption affected by using steer by propulsion?

The optimal control scheme for the concept vehicle configuration was formulated as a QP problem. This QP formulation provided solutions for the control allocation problem, which were then passed on to the individual wheel controllers. The control allocation was fed with virtual forces via the high level controllers, which used a combination of feedforward and feedback control. For simulation purposes, a reference generator was used to provide references for various test cases. Finally, all subsystems in the control system architecture were fed with data on the current state of the vehicle and the actuators, in order to gain knowledge of the actuator limitations. From simulations of the different algorithms proposed in this thesis, the final suggestion for SBP is to use the steering angle-based approach. This is due to the performance it displayed, as well as the ease of implementation. If faster yaw acceleration is requested, the desired steer angle can be used in the feedforward controller to add yaw moment that can be allocated to the rear motors.

Steer by propulsion was shown in simulation to be a viable method for controlling the steering of the vehicle. This improves redundancy in the system, increasing the safety of the vehicle. The method is able to achieve a lateral offset on a magnitude of centimeters, at lower speeds. When driving at speeds around 50 km/h or above, the performance reduces in the sense that the vehicle starts oscillating more prominently when cornering. SBP still manages to achieve lane changes at high speeds, but from a stability perspective, it is recommended to use it at lower speeds mainly.

The energy consumption comparison showed that SBP increases the consumption by 2-4 %, compared with using only power steering. Since the consumption is on par with using power steering, a suggestion would be to use SBP as a performance mode when performing more complex maneuvers. Connecting to the improved performance seen in the simulations, the performance is mainly improved at lower speeds, which is also where most complex maneuvers take place.

Since the thesis introduces several novel methods and is based on a future concept vehicle, there is naturally a lot of room for improvement. One major factor that influenced the results in this thesis, is the fact that all analyses were done completely through simulation. Thus, a natural step is to test these control schemes on a physical prototype.

In the current setup, the power steering is disabled when using SBP. However, an interesting future study would be to further analyze how the two could be combined. The first proposed torque vectoring algorithm could be used as a starting point. Since using SBP solely increases the energy consumption slightly, but also increases cornering performance, it could be combined with power steering to obtain enhanced performance at a relatively low energy cost. Increased performance could for instance be achieved by the fast response of the electric machines, which could assist in high frequency situations such as avoidance maneuvers.

Another important aspect to investigate further is the energy consumption comparison. To refine the results, more detailed models of the steering system should be used. Also additional test cases need to be explored to investigate the differences further. Since simulations showed that SBP could help improve performance and stability under certain conditions, an interesting future study could include a more detailed analysis of how the method could be used to assist in safety critical situations.

Finally, another interesting study would be to further analyze how M_{steer} affects the behavior of the vehicle. In this thesis, models of the steering system and single track models were used, and in the predecessor another method was also investigated. The conclusion is that the relation between M_{steer} and vehicle motion is rather complicated. The LQR with integral action was based on simplified models, but displayed good performance. A suggestion would therefore be to improve these models by using a system identification approach or possibly a machine learning algorithm to identify a relation between driver steer angle, normal loads and coefficient of friction.

Bibliography

[1] S. Janardhanan, L. Laine, M. Jonasson, B. Jacobson, and M. Alakula, "Concept design of electric cruise and startability axles for long haul heavy vehicles to maximise driving range." Vehicle Propulsion and Power Conference, 2021.

[2] Rivian Automotive, Inc. (2022) R1T. [Online]. Available: https://rivian.com/r1t

[3] Tesla Inc. (2022) Cybertruck. [Online]. Available: https://www.tesla.com/cybertruck

[4] C. Chatzikomis, M. Zanchetta, P. Gruber, A. Sorniotti, B. Modic, T. Motaln, L. Blagotinsek, and G. Gotovac, "An energy-efficient torque-vectoring algorithm for electric vehicles with multiple motors," *Mechanical Systems and Signal Processing*, vol. 128, pp. 655–673, 2019. [Online]. Available: https://www.sciencedirect.com/science/article/pii/S0888327019301657

[5] R. De Castro, R. E. Araújo, M. Tanelli, S. M. Savaresi, and D. Freitas, "Torque blending and wheel slip control in evs with in-wheel motors," *Vehicle System Dynamics*, vol. 50, no. sup1, pp. 71–94, 2012.

[6] Y. Wang, W. Deng, B. Zhu, Q. Zhao, and B. Litkouhi, "Allocation-based control with actuator dynamics for four-wheel independently actuated electric vehicles," *SAE International Journal of Passenger Cars-Electronic and Electrical Systems*, vol. 8, no. 2015-01-0653, pp. 425–432, 2015.

[7] B. Källstrand, "Control allocation for vehicle motion control - Maximizing traction and steering capabilities under different road conditions," Master's thesis, Chalmers University of Technology, Gothenburg, Sweden, 2017.

[8] Y. Zhao, W. Deng, J. Wu, and R. He, "Torque control allocation based on constrained optimization with regenerative braking for electric vehicles," *International journal of automotive technology*, vol. 18, no. 4, pp. 685–698, 2017.

[9] H. B. Pacejka and E. Bakker, "The magic formula tyre model," *Vehicle system dynamics*, vol. 21, no. S1, pp. 1–18, 1992.

[10] N. Hashemnia and B. Asaei, "Comparative study of using different electric motors in the electric vehicles," in *2008 18th International Conference on Electrical Machines*. IEEE, 2008, pp. 1–5.

[11] L. Laine, "Reconfigurable motion control systems for over-actuated road vehicles," Ph.D. dissertation, Chalmers University of Technology, 2007.

[12] R. Hjelte Ulmehag, "Energy management for a tractor and semitrailer combination using control allocation," Master's thesis, Chalmers University of Technology, 2016.

[13] P. Volz, "Analysis of potential in asymmetric braking for autonomous applications," Master's thesis, Chalmers University of Technology, 2018.

[14] M. Jonasson and M. Thor, “Steering redundancy for self-driving vehicles using differential braking,” *Vehicle system dynamics*, vol. 56, no. 5, pp. 791–809, 2018.

[15] G. M. Hoffmann, C. J. Tomlin, M. Montemerlo, and S. Thrun, “Autonomous automobile trajectory tracking for off-road driving: Controller design, experimental validation and racing,” in *2007 American control conference*. IEEE, 2007, pp. 2296–2301.

[16] O. Härkegård, “Backstepping and control allocation with applications to flight control,” Ph.D. dissertation, Linköping University, 2003.

[17] P. Sundström and K. Tagesson, “On real time adaptive and dynamically constrained control allocation for stability control of heavy vehicles,” Master’s thesis, Chalmers University of Technology, 2008.

[18] E.H. van den Berg, “Optimal control allocation on over-actuated vehicles,” Master’s thesis, Delft University of Technology, 2016.

[19] Y. Zhao and C. Zhang, “Electronic stability control for improving stability for an eight in-wheel motor-independent drive electric vehicle,” *Shock and Vibration*, vol. 2019, 2019.

[20] J. Pedro Marques Antunes, “Torque vectoring for a formula student prototype,” Master’s thesis, Técnico Lisboa, 2017.

[21] J. Tian, J. Tong, and S. Luo, “Differential steering control of four-wheel independent-drive electric vehicles,” *Energies*, vol. 11, no. 11, p. 2892, 2018.

DEPARTMENT OF MECHANICS AND MARITIME SCIENCES
CHALMERS UNIVERSITY OF TECHNOLOGY
Gothenburg, Sweden
www.chalmers.se

CHALMERS
UNIVERSITY OF TECHNOLOGY